


## 3D-PRINTED ELECTRODES FOR ENERGY STORAGE



# 3D-printed interdigital electrodes for electrochemical energy storage devices

Renpeng Chen<sup>1,b)</sup>, Yiming Chen<sup>1,b)</sup>, Lin Xu<sup>1,2,a)</sup>, Yu Cheng<sup>1</sup>, Xuan Zhou<sup>1</sup>, Yuyang Cai<sup>1</sup>, Liqiang Mai<sup>1,2,a)</sup> 

<sup>1</sup> State Key Laboratory of Advanced Technology for Materials Synthesis and Processing, School of Materials Science and Engineering, Wuhan University of Technology, Wuhan 430070, Hubei, People's Republic of China

<sup>2</sup> Foshan Xianhu Laboratory of the Advanced Energy Science and Technology Guangdong Laboratory, Xianhu Hydrogen Valley, Foshan 528200, Guangdong, People's Republic of China

<sup>a)</sup> Address all correspondence to these authors. e-mails: linxu@whut.edu.cn; mlq518@whut.edu.cn

<sup>b)</sup> These authors contributed equally to this work.

Received: 20 March 2021; accepted: 8 May 2021

**Interdigital electrochemical energy storage (EES) device features small size, high integration, and efficient ion transport, which is an ideal candidate for powering integrated microelectronic systems. However, traditional manufacturing techniques have limited capability in fabricating the microdevices with complex microstructure. Three-dimensional (3D) printing, as an emerging advanced manufacturing technology in rapid prototyping of 3D microstructures, can fabricate interdigital EES devices with highly controllable structure. The integration of 3D printing and interdigital devices provides great advantages in electrochemical energy storage. In this review, we discuss the common 3D printing techniques for interdigital EES devices fabrication, then the corresponding material requirements are also introduced. Recent significant research progress made in 3D-printed interdigital electrodes of batteries and supercapacitors are highlighted. Finally, to facilitate further development of 3D-printed interdigital EES devices, relevant challenges are summarized and some prospects are also proposed.**

## Introduction

Given the rapid development of wearable electronics and integrated circuits, there is increasing demand for miniaturized electrochemical energy storage (EES) devices [1, 2]. Various EES devices are transformed toward miniature, flexible, and portable ones [3–5]. Currently, batteries and supercapacitors are the most common EES devices, which can stably supply energy for various electronic systems [6–8]. Traditional batteries or supercapacitors are sandwich-like configurations, assembled by two planar electrodes, separator, and electrolyte [9]. Owing to the limitation of configuration and size, they are limited to be applied in some occasions [10]. At certain times, interdigital microdevices with highly controllable structure can overcome this problem [11]. The configuration of the interdigital structure greatly reduces the size of devices. Meanwhile, interdigital devices with narrow electrode gaps ensure efficient ion transport to provide higher power density [12]. Compared with the traditional sandwich-like EES devices, the interdigital electrode with

abundant open edges increases the contact area between active material and electrolyte, which can achieve high mass loading of active materials without affecting the ion transport between electrodes [11]. As the thickness of interdigital electrodes increases, the microelectrodes based on hierarchical ordered porous structure will provide ordered network to achieve high power density [13]. Moreover, the precise fabricating process makes the size of the devices highly controllable [14, 15]. Diversified processing technology can realize the wide application of devices, such as in integrated, wearable, and implantable electronics [16–18]. Due to the advantages mentioned above, interdigital devices have attracted a lot of attention for microelectronic systems.

Compared with traditional two-dimensional (2D) planar structure, the three-dimensional (3D) structure can achieve higher utilization of active material, more efficient ion diffusion, and lower resistance [19]. As an emerging advanced manufacturing technology, 3D printing has attracted extensive attention in recent years [20, 21]. To date, several 3D

printing technologies such as direct ink writing (DIW) [22], inkjet printing (IJP) [23], stereolithography (SLA) [24], and selected laser sintering (SLS) [25] have been used to construct electrode microstructure and regulate electrochemical performance in interdigital energy storage devices. This technique owns several significant advantages: (1) The ability to manufacture required complex structures; (2) The precise control of devices in micro-size; (3) A high degree of automation enabling large-scale production; (4) full-printed EES devices can eliminate the negative effects of different preparation processes. In general, 3D printing has great potential in the rapid manufacturing of high-performance micro-EES devices.

Previous reviews about this field mainly summarized the 3D-printed energy storage and conversion devices [26, 27], now we focus on interdigital energy storage devices. Since 3D-printed micro-interdigital devices occupy an important position in the next generation of energy storage devices due to their advantages in regulating structures and providing desirable electrochemical performance. The 3D printing of micro-interdigital devices requires consideration of the type of printing technology, material requirements, and device structure. In this review, we mainly discuss the common 3D printing techniques, corresponding material requirements, and 3D-printed interdigital batteries/supercapacitors (Fig. 1). To facilitate further research and development of 3D-printed interdigital EES devices, relevant challenges are summarized and analyzed, and some prospects are also proposed. It is believed that incorporating 3D printing into micro-EES devices can inspire more breakthroughs in the future.

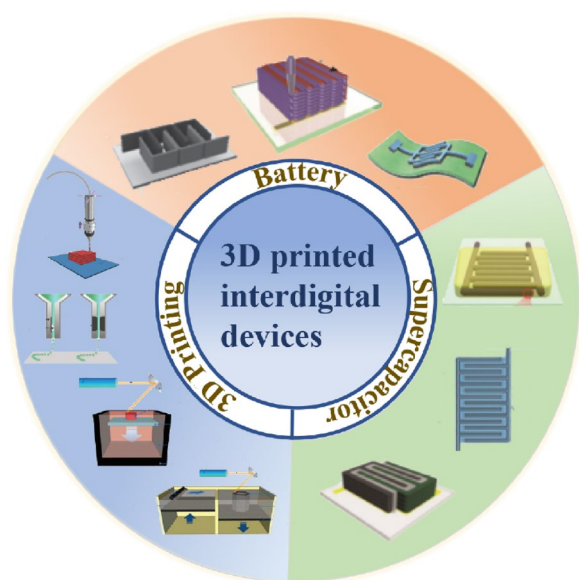


**Figure 1:** 3D-printed interdigital electrochemical energy storage devices.

## 3D printing technology for EES devices

In recent decades, many 3D printing technologies have been reported [28–30]. The geometry and texture of 3D-printed batteries and supercapacitors can be accurately controlled by greatly automated and economical processes of 3D printing [31, 32]. However, considering the unique advantages of different printing techniques, it is important to use appropriate 3D printing techniques to manufacture microdevices with different structures. The interdigital EES devices are commonly fabricated by DIW, IJP, SLA, and SLS printing methods, corresponding 3D printing techniques are shown in Fig. 2 [33, 34]. This section mainly introduces these printing techniques, including the manufacturing process, material requirements, and involved advantages/disadvantages.

### Direct ink writing

DIW is an additive manufacturing technology widely used in 3D printing batteries and supercapacitors due to its advantages of low cost, convenient operation, and diverse material options [35]. The inks are deposited on the various substrate through a nozzle, which is controlled by the digital procedure (Fig. 2a). The ink filaments are usually extruded out at room temperature, and the latter layer is deposited on the former layer by moving the nozzle to create a 3D structure. Meanwhile, the composition and rheological property of the ink is the key factors to achieve continuous filaments. The great shear-thinning behavior is vital for printing inks, that is, the viscosity decreases with the increase of shear rate. The low viscosity at a high shear rate is conducive to the smooth extrusion of the inks, and then the inks deposited on the substrate will restore solid behavior due to the disappearance of shear force. Therefore, a layered structure with controllable thickness is created.

### Inkjet printing

IJP is a direct material jet technology (Fig. 2b), which can use a commercial inkjet printer to print inks on paper or other substrates to create predesigned patterns [36]. There are some apparent strengths in IJP, including common printing equipment, facility process, fast and economical materials deposition. The key challenge to IJP printing is the extrusion adaptability of inks, low-viscosity inks consisting of actives materials are usually used for subsequent printing. Although a small amount of material is consumed in the printing process, the printing of thick electrodes is difficult when using low-viscosity inks. Carbon-based materials, polymer, and metal can be deposited on different substrates by inkjet printing. Interdigital supercapacitors have been already printed on conventional A4 paper by IJP [37]. At first, to obtain high-resolution images, cellulose nanofibers (CNF)-based nanomaterials were printed onto A4

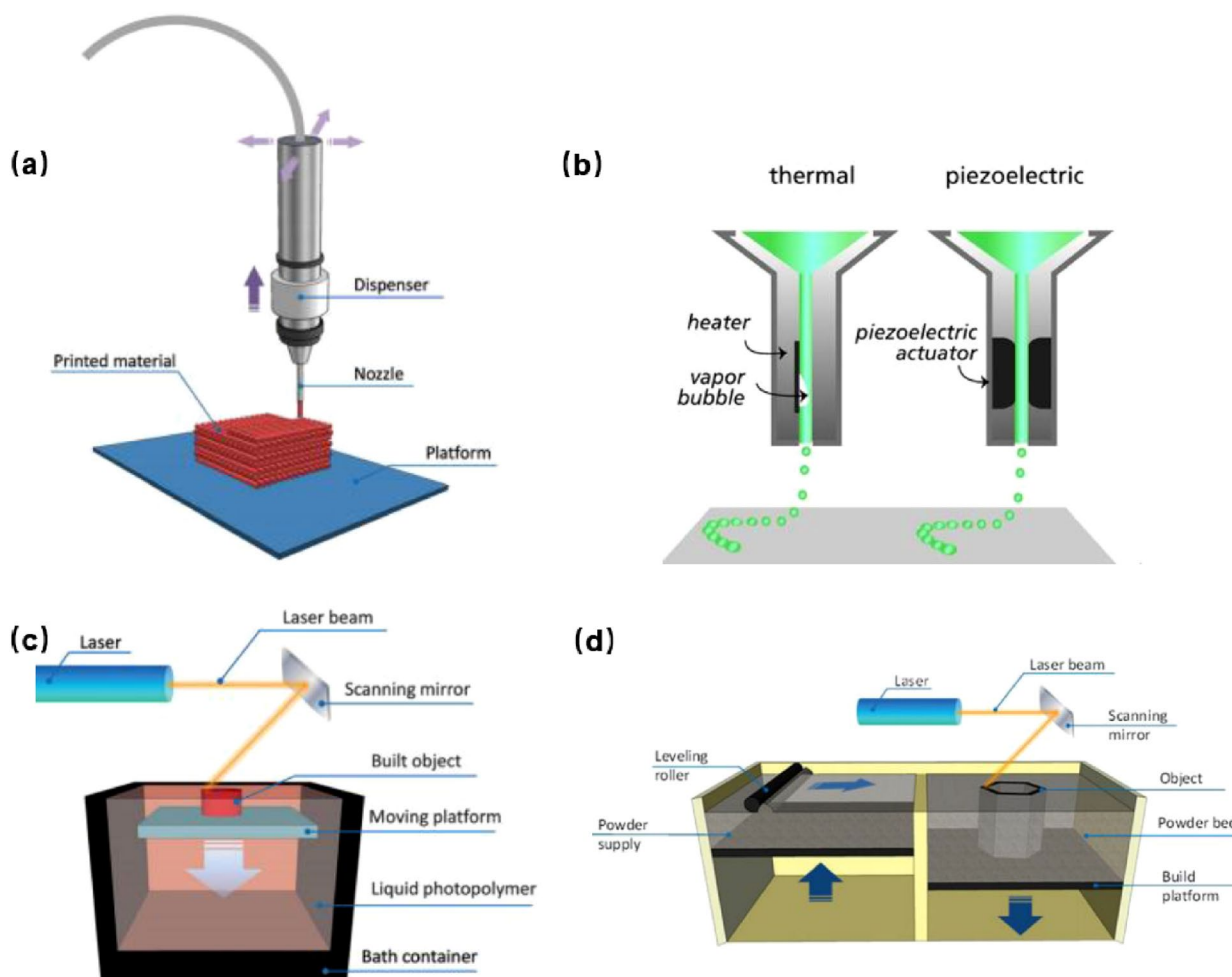


**Figure 2:** Various 3D printing techniques. (a) DIW is a layer-by-layer process of depositing the ink material. Adapted from Ref. [33]. (b) In IJP, inks are deposited on substrate. Adapted from Ref. [34]. (c) SLA uses the photopolymer. (d) SLS uses a laser to sinter or fuse the powder particles. Adapted from Ref. [33].

paper by IJP. The inks of the electrodes were composed of activated carbon, carbon nanotube (CNT), and Ag nanowire. Delicate interdigital symmetrical electrodes were inkjet printed on CNF treated A4 paper. The assembled supercapacitor showed capacitance of about  $100 \text{ mF cm}^{-2}$  at  $0.2 \text{ mA}$ , and there was almost no decrease in the capacitance over 10,000 cycles.

### Stereolithography

SLA is rapidly popularized in the field of printing energy storage devices because of its high degree of automation, high dimensional accuracy, and accessible processing [38]. Generally, ultraviolet (UV) photocurable resin is the necessary material in the SLA printing method. Figure 2c shows the SLA preparation process, a light source of a specific wavelength and intensity is used to irradiate the printed photocurable material. After the photocurable resin is irradiated by a light source, a cross-linking reaction occurs and a solidified layer is formed by sequential irradiation from point to line to surface. Then the lifting platform

moves vertically to another layer height, and the printer repeats the irradiation steps so that a geometry structure is constructed layer by layer [39]. DIW and IJP, based on direct extrusion, are limited by the printing paths and layers. Moreover, there are obvious advantages of the SLA method in printing microstructure devices. This printing technology can even print very complicated hollow structures. However, the shortcomings of SLA are also obvious, including expensive equipment and maintenance costs, high requirements for a working environment, and long preparation durations. Therefore, developing more simple and low-cost SLA technology is a significant research direction in the future.

### Selective laser sintering

Selective laser sintering is an advanced 3D printing technology originally proposed by Carl. R. Deckard of the University of Texas at Austin in 1986 [40]. Pure ceramics, metals, polymers, carbon material powders, or mixed powders can be directly used

for SLS printing without additional material processing. The production can be fabricated by melting all or some part of the powders by laser irradiation. In the manufacturing process, the powders are spread on the printing platform and then melted by a laser to achieve one-layer printing. Once the first layer printing finishing, the platform will descend to another plane for reloading powders, and then stacked layer by layer by thermoforming to form a 3D device (Fig. 2d). Polymers with low melting points can be incorporated into other materials such as carbon during printing processing. The melted materials will spread on the surface of other solid particles to connect them as a binder, which further improves the electrochemical performance [41, 42]. A wide range of materials can be used in SLS, but the high cost restricts the application in the field of energy storage.

The fabrication process of the different 3D printing method is summarized here. Each method has its own strengths and limitations. Table 1 summarizes the advantages and disadvantages of 3D printing. According to the different materials requirements for printing technology, the appropriate materials are key factors to manufacture high-performance devices. 3D Printing methods based on extrusion or inkjet process, such as DIW and IJP, feature diverse materials option, low cost, and no special condition requirements. It has the largest flexibility in directly printing inks on various substrates. However, because of the limitation of the printing path, it is difficult to prepare a high-precision 3D microstructure. The devices with complex structures can be achieved by SLA and SLS. Nevertheless, the disadvantages of SLA and SLS are also obvious. SLA printing is limited to UV curing materials and a long curing period. SLS is not limited by extrusion ink or UV curable materials, but the high printing cost hinders its large-scale application. Many novel 3D printing technologies have been reported [43], and the development of new 3D printing technologies and optimization of existing methods still require great effort.

### Material requirements for 3D-printed EES devices

EES devices such as batteries and supercapacitors are generally composed of cathode, anode, electrolyte, collector, and packaging. Compared with the traditional preparation technology, 3D printing has its unique strengths in the preparation of various

components of EES devices, especially in the preparation of full-printed devices. In the extrusion-based process, the composition of inks is critical to obtain the ideal performance of EES devices. The viscosity of qualified printing ink must be controllable, which can be achieved by adjusting the configuration and proportion of raw materials. Meanwhile, the choice of ink solvent is also very important. Different solvents will directly affect the dispersion of ink components. In the process of printing, the stable inks with high storage modulus realize continuous extrusion and structural integrity.

### Electrode materials

Traditional electrode materials usually include active materials, conductive additives, and binders. The planar electrode is fabricated by a 2D planar preparation process such as coating and calendaring. The diversity of 3D printing technology makes the manufacturing of different electrode materials more flexible. Different materials, such as inorganic materials, carbon materials, polymers, UV curable resins, need to be processed with appropriate 3D printing technology. Conductive carbon-based materials and their composites can be directly used as active materials or conductive carriers for electrodes. Some porous inorganic semiconductor materials such as oxides can provide unique electrochemical reactivities. Insulating polymer materials can be used as templates/supports [44]. Compared with traditional electrode slurry, the electrode inks are more complex. Active materials for 3D-printed electrodes mainly include  $\text{LiCoO}_2$  (LCO) [45],  $\text{LiTi}_5\text{O}_{12}$  (LTO) [46],  $\text{LiFePO}_4$  (LFP) [47], and polyaniline (PANI) [48], etc. The electrode material inks are the key to the preparation of EES devices electrodes in 3D printing. Hu et al. optimized the performance of  $\text{LiFePO}_4$  by carbon coating and manganese doping to prepare the  $\text{LiMn}_{1-x}\text{Fe}_x\text{PO}_4@\text{C}$  composite slurry. The capacity of the printed electrodes was up to  $108 \text{ mAh g}^{-1}$  at high rate of 100 C, and the high capacity of  $150 \text{ mAh g}^{-1}$  can be maintained at 10 C after 1000 cycles [49]. Cai et al. fabricated sulfur/carbon/ $\text{LaB}_6$  cathodes with ample hierarchical pores for Li-S batteries, which exhibited high areal capacity of  $7.98 \text{ mAh cm}^{-2}$  at a sulfur loading of  $9.3 \text{ mg cm}^{-2}$  [50]. In addition, the additive such as graphene oxide (GO) [51, 52], polymers [53], cellulose [22, 54, 55], or nanomaterials [28, 56] are often added to inks to

**TABLE 1:** Summary of advantages and disadvantages of 3D printing.

Technique	Materials	Advantages	Disadvantages
DIW	Polymer; ceramic	Low cost; high speed; complex architectures; wide choice of materials	Ink requirement of specific rheology
IJP	Polymer; ceramic	Low materials waste; facility process	Limited choice of inks
SLA	Photopolymers	High printing resolution; complex architectures	High cost; limited choice of materials
SLS	Polymer; ceramic, metals	High printing resolution	Very high cost



regulate the rheological properties. GO has been widely used in printing inks as the active materials and additives. In addition to improving the rheological properties of inks, the GO with abundant functional groups also provides large number of reaction sites, which are suitable for the preparation of high-performance hybrid inks. Liu et al. [57] prepared composite inks by in situ growth of vertically aligned PANI on GO surface to prepare interdigital micro-supercapacitor (MSC). The fabricated MSC showed high areal capacitance ( $153.6 \text{ mF cm}^{-2}$ ) and outstanding capacitance retention (100%) after 5000 cycles.

### Electrolyte materials

Due to the special structure of interdigital electrodes, a separator is not required between two electrodes. There is a narrow gap in the interdigital electrodes, and the electrolytes can be accurately printed between the two electrodes through the nozzle [58] (Fig. 3a–c). This precise printing not only increases the energy density of EES devices but also reduces the waste of materials. At present, the polymer [59, 60], ionic liquid [61, 62], and solid electrolyte [63, 64] have been successfully applied in 3D printing. Gel polymers are often used as the electrolytes of 3D-printed batteries or supercapacitors. It can be solidified on electrodes through solvent evaporation, photopolymerization, and thermal polymerization. The electrolytes can be assembled into EES devices by pouring, infiltrating, and injecting. To further explore the full-printed high-performance devices, electrolytes based on ionic liquids are also used for 3D printing. On the one hand, ionic liquids provide high working voltage to improve the energy density and power density of EES devices; on the other hand, their outstanding high-temperature resistance improves the working safety [65]. Moreover, solid electrolytes, with their high safety and mechanical stability, could be a powerful alternative to liquid electrolytes. However, solid electrolytes generally have the disadvantages of high contact resistance and low ionic conductivity [66]. Solid-state electrolytes with various structures processed by 3D printing can effectively improve this problem. McOwen et al. [67] printed  $\text{Li}_7\text{La}_3\text{Zr}_2\text{O}_{12}$  (LLZO) solid electrolytes with various microstructures by DIW method. The rheological properties of inks greatly affect the configuration and microstructure of the printed electrolyte. Nano-size LLZO particles were mixed with two different binders system to form the ink. One was a Polyvinyl butyral (PVB) binder with benzyl butyl phthalate (BBP) plasticizer and the other was texanol-based composition. The inks composed of the former binder system had conformal nature, while the latter exhibited high self-supporting ability. The authors used these two inks to print solid electrolytes with different structures, such as lines, grids, and columns (Fig. 3d–i). Finally, they filled lithium electrodes on both sides of the printed LLZO grids (Fig. 3j, k). Due to the close electrode–electrolyte contact, a low interface impedance of  $38 \Omega \text{ cm}^2$  was obtained. Furthermore,

the symmetrical cell exhibited stable and low overpotential at different current densities.

### Current collector materials

The current collector gathers the active material into a whole, and the current generated by it is collected to form a larger external output. Therefore, the current collector should fully contact the active material. Traditional planar current collectors, such as metal foil, cannot provide a larger contact area for electrode materials due to structural limitations. 3D printing technology can print the collector with a highly controllable microstructure, which can provide a larger contact area. Compared with the metal planar collector, higher performance materials can be directly printed in energy storage devices. Chae et al. [68] printed nickel nanoparticles-based interdigital collector by flash light stringing technology. The fabricated supercapacitor with carbon-based electrodes on the nickel collector exhibited high area energy density ( $12.8 \text{ mW cm}^{-2}$ ) at voltage up to 3 V. It should also be noted that electrodes printed directly by doping with highly conductive metal particles could eliminate the current collector [69]. The removal of the inert part is beneficial to the miniaturization of the EES devices and the higher proportion of active materials makes higher energy density.

### Packaging materials

Tremendous works are focused on printing electrodes and electrolytes. However, suitable 3D-printed packaging materials are also crucial for energy storage devices. According to the form of printed electrodes, it can be packaged in the form of a button or a soft pack. For interdigital devices, packaging materials such as polyethylene terephthalate (PET) film, polydimethylsiloxane (PDMS), and other polymer resins are often used for packaging [70]. This method, involving inaccurate processes such as transfer, alignment, and a package of printed patterns, reduces the repeatability of EES devices. To fabricate more accurate energy storage devices, suitable packaging strategies for various shapes and sizes are required. Package materials are quite different from the materials used in functional parts such as electrodes and electrolytes. Chen et al. [71] printed a fully packaged supercapacitor through DIW technology. CNT-based electrodes, PVA gel electrolyte, and silicone packaging were printed on a flexible polyimide substrate in sequence. The packaged supercapacitor had capacitance retention of 97.7% after 1000 cycles, indicating that there is no obvious negative effect on electrochemical performance. In addition, UV curable composite inks were also produced to manufacture fully 3D-printed EES devices [72].

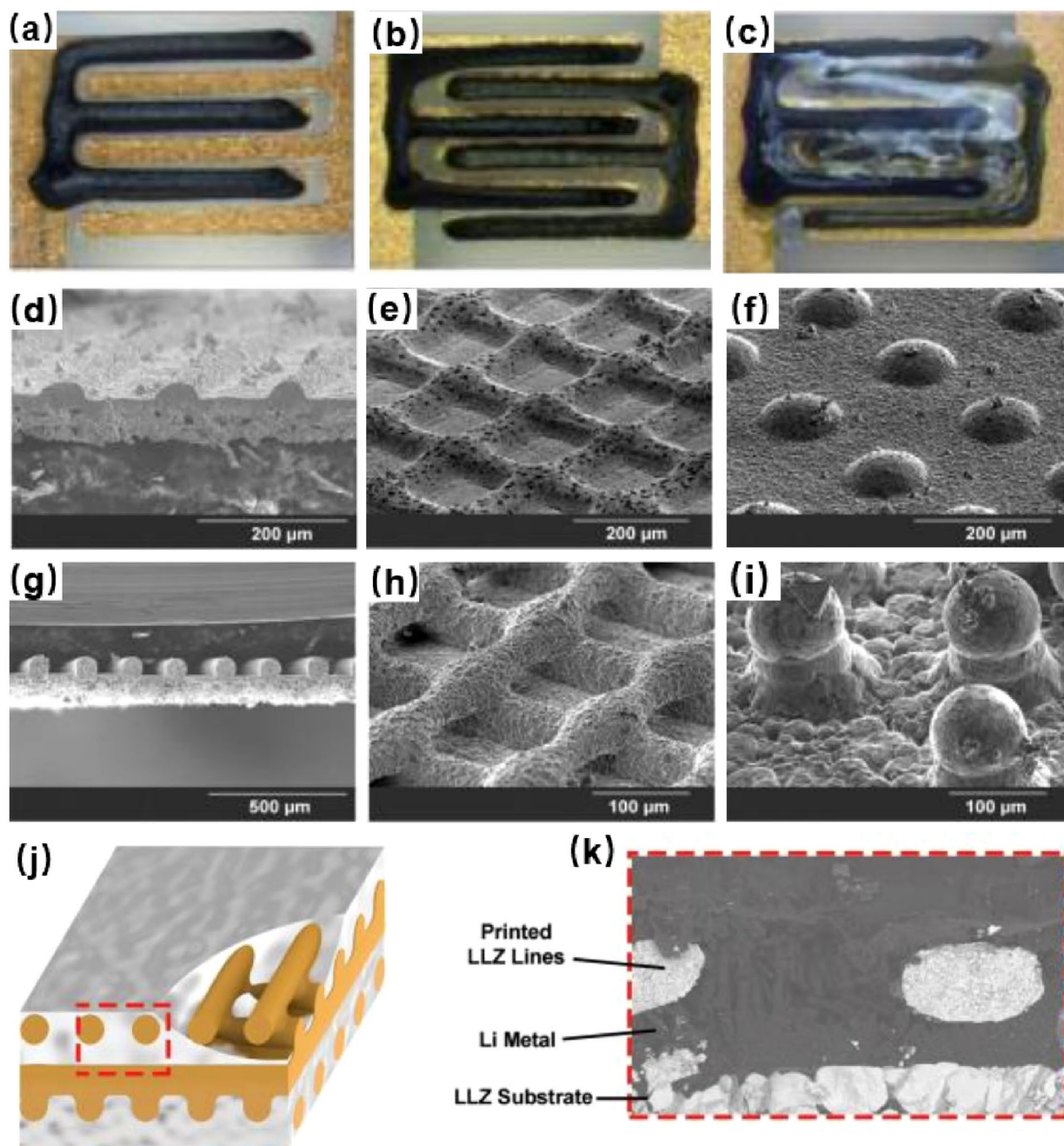


**Figure 3:** (a–c) Digital photograph of gel electrolyte printed accurately into two electrodes. Adapted from Ref. [58]. (d–f) SEM images of printed different structures using conformal ink, and (g–i) self-supporting ink. (j) Schematic diagram of printed LLZO grids filled by Li metal. (k) SEM images of the interface between LLZO lines and Li Metal. Adapted from Ref. [67].

### Application of 3D-printed interdigital EES devices

3D printing technologies can produce energy storage devices with various architectures [44, 49, 51, 73] which provide a huge advantage for preparing EES devices with improved performance. Among them, the highly controllable interdigital structure is suitable for various micro-integrated devices.

Meanwhile, 3D printing can also introduce geometric structure into battery and supercapacitor materials, which overcomes the planar limitations. This section mainly focuses on the research progress of 3D-printed interdigital electrodes of batteries and supercapacitors, including the printing process, the composition of printing inks, and relevant electrochemical properties.

**Batteries**

LiFePO<sub>4</sub> (LFP) and Li<sub>4</sub>Ti<sub>5</sub>O<sub>12</sub> (LTO) are respectively commonly used cathode and anode materials in lithium-ion batteries. In 2013, Sun et al. [74] fabricated electrode inks composed of deionized water, ethylene glycol, glycerol, cellulose-based viscosifiers, and electrode materials (LFP or LTO). The electrode inks were deposited on the glass substrate through extrusion-based 3D printing methods to fabricate multilayered interdigital electrodes via layer-by-layer deposition, the printing process is shown in Fig. 4a. It is worth noting that the water in the inks will evaporate during the high-temperature printing process, which promotes the curing of the inks. At the same time, ethylene glycol and glycerin with high boiling points will remain as humectants, resulting in overall shape retention. Then the printed electrode was sintered in an inert gas at 600 °C to remove the organic solvent, and a porous electrode material was obtained (Fig. 4b, c). The resistance of the LFP and LTO films measured with a four-point probe was  $2.3 \times 10^3 \Omega \text{ cm}$  and  $2.1 \times 10^5 \Omega \text{ cm}$ , respectively. The printed micro-battery was also packaged by polymer material (Fig. 4d). The assembled full cell with 8-layer printed electrodes exhibited a unit areal capacity of 1.5 mAh cm<sup>-2</sup> below 5 C (Fig. 4e). In generally, the high surface energy makes the electrolyte have a small contact angle with the

solid surface, and the electrodes will be wet better by electrolyte. However, the conductivity of the ink without conductive additives did not meet the requirement. To improve the electrochemical performance of the battery, it is universal to add highly conductive materials to the inks. Fu et al. [47] added GO into printing inks as a conductive additive for the first time, LFP/GO and LTO/GO acted as negative and positive materials to prepare interdigital electrodes (Fig. 4f-h). The addition of GO improved the shear-thinning behavior of the inks, and GO flakes could align well under the shear stress of the nozzle. This work also explored the effect of GO content on the rheological properties of the ink. There was little effect on inks with the addition of LFP or LTO powders when concentration was maintained at 80 mg ml<sup>-1</sup>, showing relatively stable viscosity retention (Fig. 4i). The printed electrode was freeze-dried and then treated at a high temperature of 600 °C, a reduced graphene oxide (rGO) hybrid electrode with high conductivity was obtained. The electrical conductivities of LFP/rGO and LTO/rGO were 31.6 and 6.1 S cm<sup>-1</sup>, respectively.

There are a few reports on 3D printing lithium metal batteries with metal lithium as an anode. Cao et al. [54] prepared a porous lithium metal anode by infusing molten Li metal into a 3D-printed CNF frame (Fig. 5a). There were abundant hydroxyl

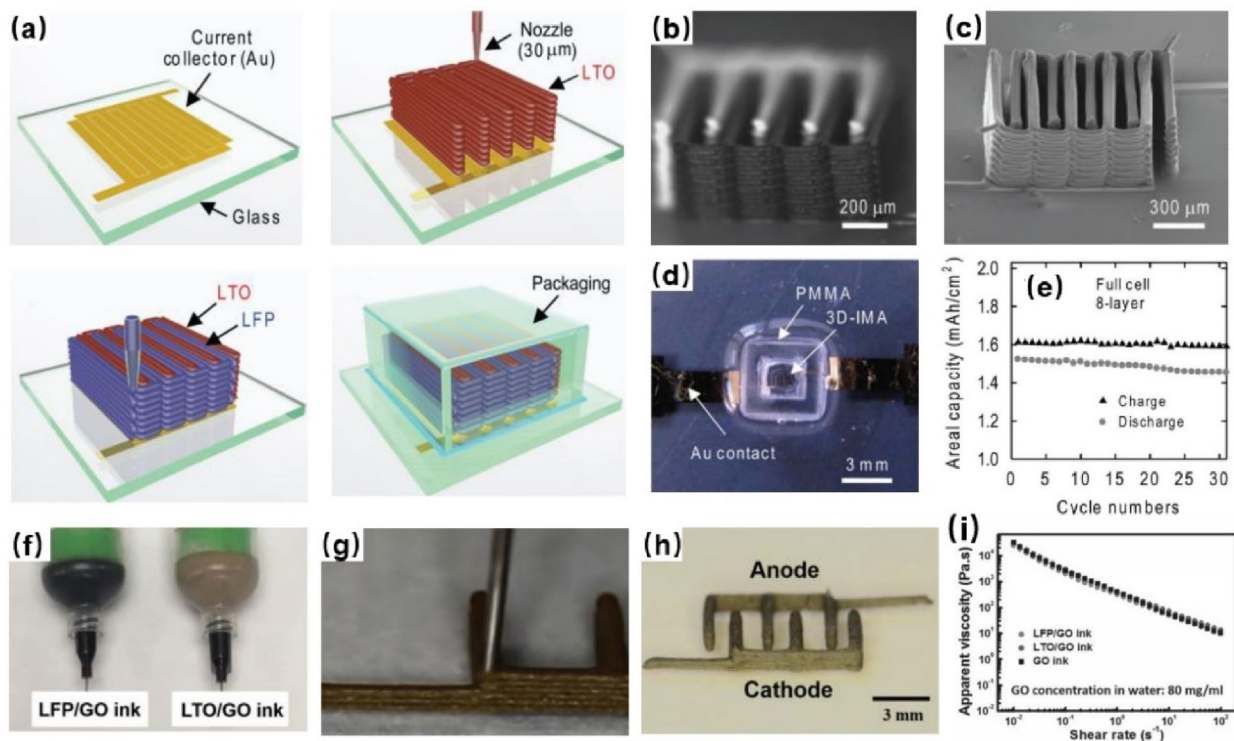


**Figure 4:** (a) Schematic illustration of the 3D printing interdigital Li-ion battery. (b) Optical and (c) SEM images of 3D-printed interdigital LTO-LFP electrode. (d) Optical images of the packaged micro-battery using PMMA packaging materials. (e) Cycling performance of 8-layer LTO-LFP electrode full cell for 30 cycles. Adapted from Ref. [74]. (f-h) Optical images of the LFP/GO and LTO/GO ink, and the interdigital electrode was printed using LFP/GO and LTO/GO ink. (i) Apparent viscosity as a function of shear rate for GO-based inks, including GO, GO/LFP, and GO/LTO. Adapted from Ref. [47].



groups on the surface of CNF, which were bonded together through strong hydrogen bonds, showing high water-retaining ability. Figure 5b shows the optical photographs of different CNF-based inks. Figure 5c and d shows the printed layer by filament CNF/LFP cathodes. Owing to the outstanding characteristic of CNF, the addition of it could improve the viscosity and shear-thinning property of inks. The printed CNF frame also had high structural integrity and water-retaining ability. After removing the water, a porous electrode would be obtained, resulting in the efficient transport of Li ions. The CNF anode infused with Li metal (c-CNF/Li) was assembled as a symmetrical cell for cycling testing. The symmetrical cell tested at a high current density of  $5 \text{ mA cm}^{-2}$  showed only 0.05 V overpotential (Fig. 5e). The porous structure with a large surface area facilitated the transport of Li ions, and no obvious lithium dendrites appeared in the c-CNF/Li electrode after cycling, which was

contrary to the Li metal with stronger dendrites (Fig. 5f-i). Besides, 3D printing lithium salt (LiF) [75] and lithium metal inks [76] that can be written directly have been reported, which might be promising materials for Li anode printing in the future.

Various functional polymers are also commonly used in inks. Rocha et al. [77] used thermal responsive inks to print electrode materials and copper current collector. The author developed the thermal responsive electrode inks which was mixed with polymer Pluronic F127 and chemically modified graphene (CMG). At temperatures below the lower critical solution temperature (LCST), this ink showed lower viscosity and liquid behavior, while it showed high viscosity and curing behavior at temperatures higher than the LCST. In addition to the heat-sensitive properties, the ink formulated by CMG and Pluronic F127 at a ratio of 1:1 showed good rheology. When the CMG content was 6 wt%, the inks showed a storage

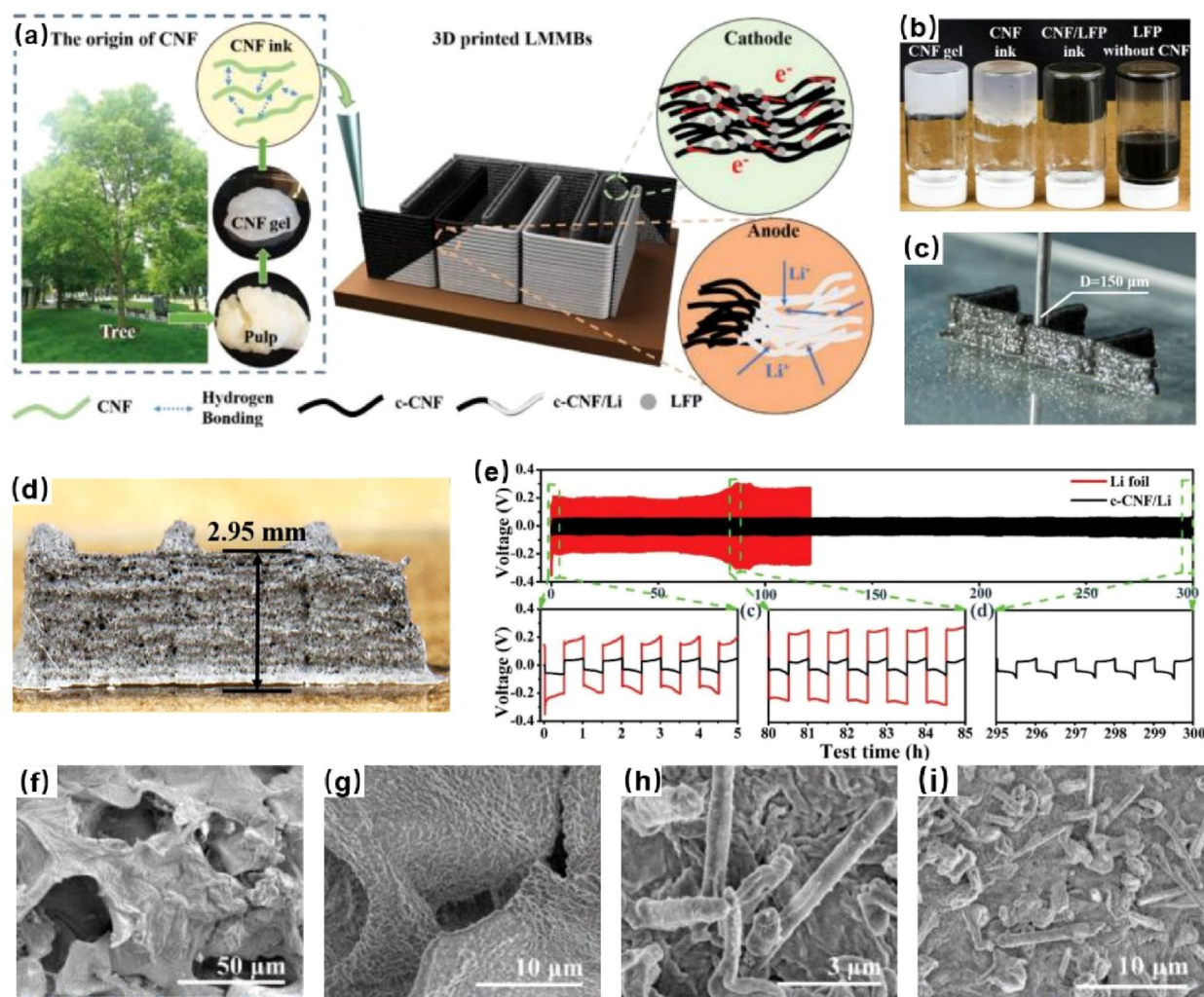


**Figure 5:** (a) 3D-printed Li metal battery with c-CNF/LFP cathode and c-CNF/Li anode. (b) Optical images of CNF gel, CNF ink, CNF/LFP ink, and LFP ink without CNF. (c) Printed CNF/LFP interdigital layer cathode, and (d) dried 15 layers CNF/LFP electrode. (e) Cycles life of symmetric cell at  $5 \text{ mA cm}^{-2}$  and  $2.5 \text{ mAh cm}^{-2}$  for 300 h. (f) and (g) SEM images of c-CNF/Li with porous structure and smooth surface after cycling; (h) and (i) SEM images of pure Li foil with dendrites after cycling. Adapted from Ref. [54].



modulus of 100 K pa. This thermal responsive ink could be applied to a broad range of carbon, metal, ceramics, and other materials, opening new possibilities for the printing of energy storage devices. UV curable resins can be used in the SLA manufacturing process. Chen et al. [24] printed poly(ethylene oxide) (PEO)-based electrodes and electrolytes by SLA. PEO is commonly used in electrolyte and binder materials for lithium-ion batteries [78]. Because of its photocurable properties, it could be used in the SLA printing process [79]. In this work, the electrode inks were composed of PEO-based resin, carbon black, and LTO or LFP (as anode and cathode active materials, respectively). In addition to providing photocurable characteristics, the PEO polymer could also provide conductive channels to increase the ionic conductivity. In particular, the degree of curing could be regulated by changing the content of photo initiator in the resin. Thereby the ideal thickness and mechanical properties of printed electrodes were obtained. Finally, the zigzag electrodes were printed and assembled to

an interdigital structure micro-battery with an areal capacity of  $1.4 \mu\text{Ah cm}^{-2}$ .

Liu et al. [25] fabricated interdigital graphite electrodes for dual ion micro-battery (DIMB). The preparation process of the micro-battery is shown in Fig. 6a. Firstly, the graphite was evenly coated on the aluminum substrate, then the micro-interdigital electrodes were directly printed via laser direct writing. Finally, the quasi-solid electrolyte soaked in the  $\text{LiPF}_6$  solution was covered on the surface of the interdigital electrodes. The length and width of the graphite interdigitated electrodes were only 3 mm and 0.5 mm respectively, and a unite DIMB area was less than  $0.75 \text{ cm}^2$  (Fig. 6b). The DIMB assembled by graphite electrodes exhibited a high capacity of  $56.50 \text{ mAh cm}^{-3}$  at 1 C and excellent cycling stability with 70% capacity retention after 700 cycles under high working voltage (Fig. 6e). It was worth noting that the DIMB had high integration and the devices can be connected in parallel or series (Fig. 6c, d). 20 DIMBs were connected in series with a discharge voltage up to 100 V (Fig. 6g).

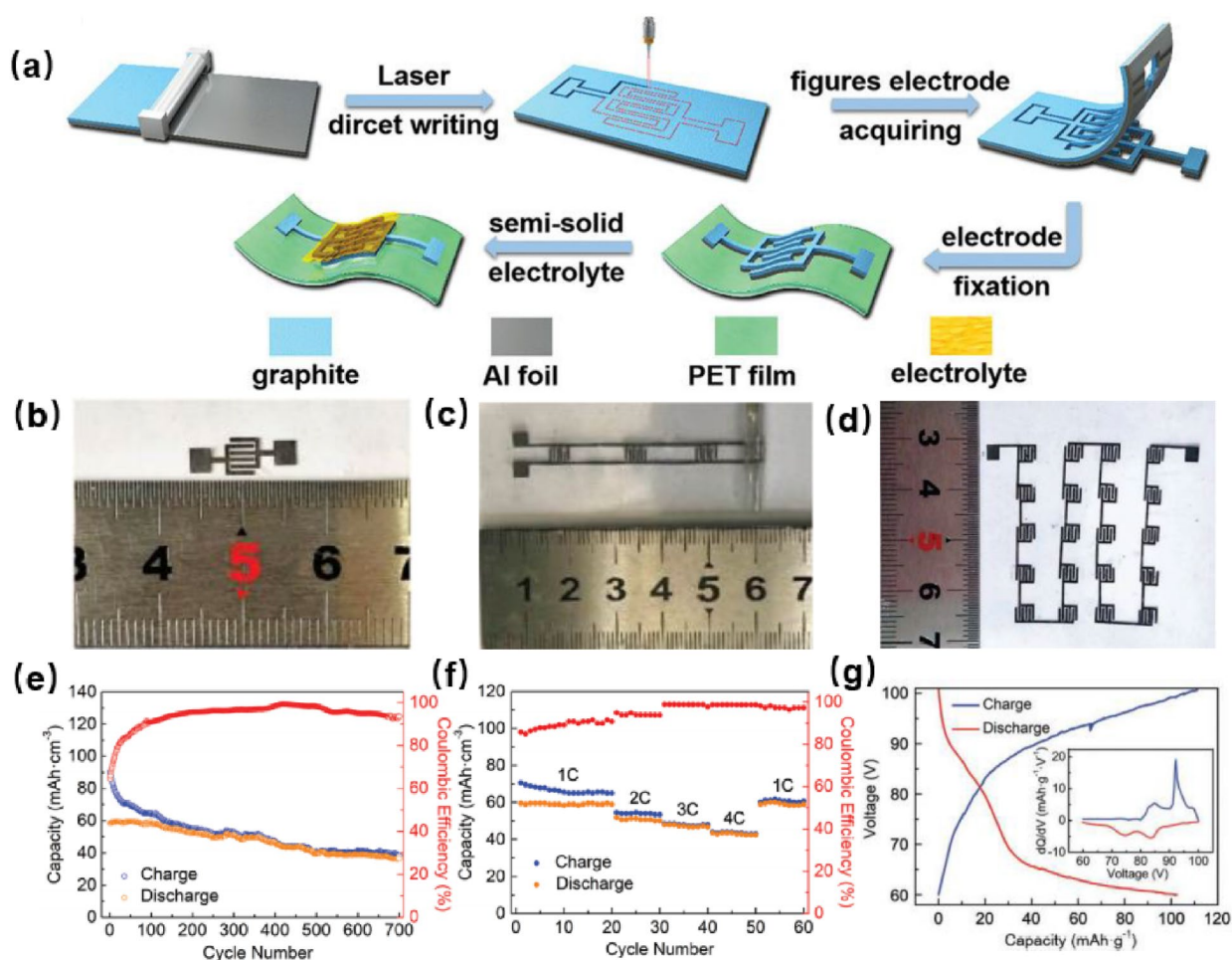


**Figure 6:** (a) Schematic illustration of the interdigital graphite electrodes fabricated via SLS technology. (b) Optical images of a DIMB with less than  $0.75 \text{ cm}^2$ . (c) Optical images of multiple DIMBs connected in parallel. (d) Optical images of 20 DIMBs connected in series. (e) Cycling life of DIMB at 1 C. (f) The rate capability of DIMB. (g) The charge and discharge curves of 20 DIMBs with a high voltage of 100 V. Adapted from Ref. [25].

This work also studied the application of DIMB in many micro-devices, including light-emitting diodes, digital game consoles, electrochromic glasses.

In the context of electronic equipment constantly upgrading to miniaturization and high-frequency, the miniaturized and integrated energy storage devices with superior electrochemical performance will naturally become an essential part of micro-electronic systems. Table 2 summarizes the materials and electrochemical performances referring to recently published papers about printed interdigital batteries. Although some progress on 3D-printed interdigital batteries has been made, there are few studies on the degradation mechanism of their electrochemical properties. At present, in situ characterization techniques have been used to track the working state of devices [80]. It is necessary to combine in situ techniques with 3D printing in the future. Meanwhile, the high matching of processes, materials, and structures also need to be explored in depth.

### Supercapacitors

With the development of miniaturized and wearable electronics, it is urgent to develop advanced flexible MSC [82]. It is a feasible idea to fabricate 3D printing devices on the flexible substrate, but direct printing of electrode patterns on the flexible substrate is not adequate. Extensive efforts should be devoted to preparing electrodes with mechanical robustness. Rajendrana et al. [83] prepared stretchable electrodes with polyurethane as a stretchable binder and CNT/PANI as active materials. The inks were printed on copier paper treated by starch aqueous solution, and then the printed electrodes were transferred to the elastic substrate to prepare stretchable electrodes with free-standing serpentine interconnects. The combination of intrinsic stretchable ability and free-standing serpentine interconnects structure of electrodes was an efficient means for realizing highly stretchable MSC. After bending and twisting testing, the specific capacitance of the fabricated supercapacitor still maintained more than 90%. Meanwhile, the interdigital device showed 167 mF cm<sup>-2</sup> areal capacitance at a current density of

0.4 mA cm<sup>-2</sup>. In addition to being able to withstand a certain tensile strain, a high unit areal capacitance is required to provide high power in limited space. Li et al. [84] used 3D printing and the unidirectional freeze-drying method to prepare interdigital electrodes. The directional honeycomb porous structure inside the electrodes greatly improved the areal capacitance of MSC, and it also provided high mechanical properties while the electrode was thick. The used inks consisted of manganese dioxide nanowires (MnONWs), silver nanowires (AgNWs), fullerene (C60), and Ti<sub>3</sub>C<sub>2</sub>T<sub>x</sub> (the most studied 2D materials). A conductive 3D network was provided by highly conductive AgNWs and high areal capacitance was attributed to oriented MnONWs and MXene, while C60 could reduce the friction between layered electrodes and further improve the tensile stability of thick electrodes. The fabricating process of interdigital MSC with a honeycomb porous structure is shown in Fig. 7a. Firstly, the inks were printed on the PDMS flexible substrate, and then the honeycomb porous electrode structure was achieved by unidirectional freezing and freeze-drying. As shown in Fig. 7b and c, the electrodes with parallel honeycomb porous microstructure were clearly present. The areal capacitance, energy density, and power density of the fabricated MSC was as high as 216.2 mF cm<sup>-2</sup>, 19.2 μWh cm<sup>-2</sup>, and 58.3 mW cm<sup>-2</sup>, respectively. It was worth noting that no obvious damages appeared in MSC after stretching or bending, and electrochemical performance of the MSC was still maintained well (Fig. 7d–g).

Supercapacitors have been great affected by the contact area of electrolyte and electrode [85]. Electrolyte and electrode with multiple microarchitectures can be constructed by 3D printing to obtain increased surface area [86]. Recently, 2D materials have been widely used in 3D-printed supercapacitors [87–90]. As innovative materials, MXenes (2D transition metal carbides) with a high specific surface area can be used in electrodes materials to create MSC with excellent electrochemical performance [91, 92]. Yang et al. [93] used Ti<sub>3</sub>C<sub>2</sub>T<sub>x</sub> to print MSC interdigital electrodes without current collectors. The Ti<sub>3</sub>C<sub>2</sub>T<sub>x</sub> sheets with an average horizontal size of 8 μm and thickness of 1–3 nm were prepared. At a lower concentration (15 mg mL<sup>-1</sup>), the viscosity

**TABLE 2:** Various types of inks prescribed and the electrochemical performances of the printed interdigital battery.

Cathode/anode	Electrolyte	Specific capacity	Energy/power density	References
LFP/LTO	1 M LiClO <sub>4</sub> EC:DMC 1:1	1.2 mAh cm <sup>-2</sup> at 0.5 C	9.7 J cm <sup>-2</sup> at 2.7 mW cm <sup>-2</sup>	[74]
(LFP-rGO)/(LTO-rGO)	PVDF-co-HFP and Al <sub>2</sub> O <sub>3</sub>	91 mAh g <sup>-1</sup> at 50 mA g <sup>-1</sup>		[47]
LFP/LTO	PEG and 1 M LiClO <sub>4</sub> (EC: PC 1:1)	1.4 μAh cm <sup>-2</sup>		[24]
(c-CNF-LFP)/(c-CNF-Li)	1 M LiTFSI DOL:DME 1:1 with 2 wt% lithium nitrate	80 mA h g <sup>-1</sup> at 10 C		[54]
MnO <sub>2</sub> @NCAs/Zn@NCAs	ZnSO <sub>4</sub> and MnSO <sub>4</sub>	30.29 μAh cm <sup>-2</sup> μm <sup>-1</sup> at 6 C	71.3 μW h cm <sup>-2</sup> at 69.5 μW cm <sup>-2</sup>	[16]
MnO <sub>2</sub> /Zn	ZnSO <sub>4</sub> and MnSO <sub>4</sub>	253.8 mAh g <sup>-1</sup> at 0.5 A g <sup>-1</sup>		[17]
Graphite/graphite	LiPF <sub>6</sub>	56.50 mAh cm <sup>-3</sup> at 0.165 mA cm <sup>-2</sup>	291.1 mWh cm <sup>-3</sup> at 1 C	[25]
Si–C-graphite/Li	1 M LiPF <sub>6</sub> EC: DMC 1:1 with 10 wt% FEC	466 mA h g <sup>-1</sup> at C/4		[81]

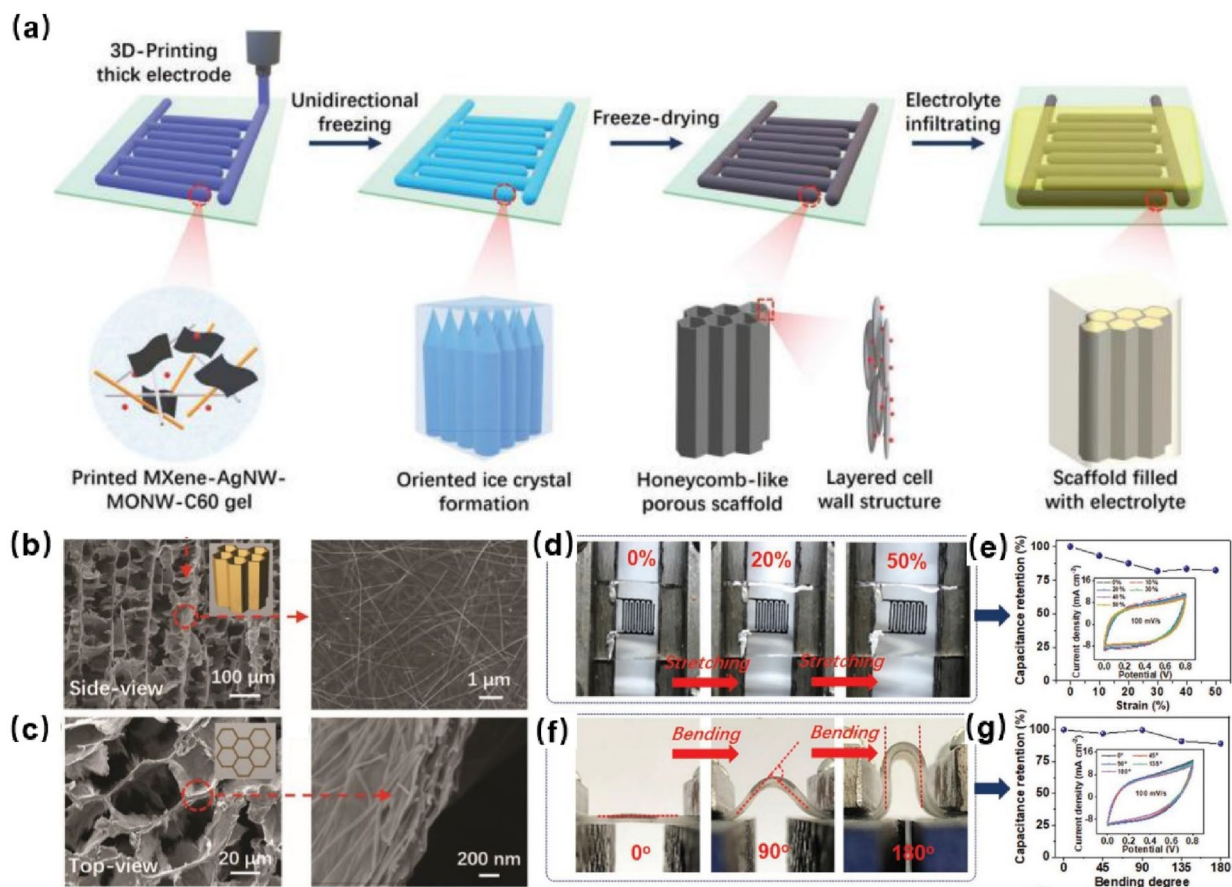


**Figure 7:** (a) Schematic illustration of the preparation route of the 3D-printed micro-supercapacitors via unidirectional freezing. (b) A honeycomb-like scaffold of finger electrode in side-view, and (c) in top-view. (d) Optical images of MSC under stretching 0% to 50%. (e) Capacitance retention and CV curves at  $100 \text{ mV s}^{-1}$  under different stretching degree. (f) Optical images of MSC under bending  $0^\circ$  to  $180^\circ$ . (g) Capacitance retention and CV curves at  $100 \text{ mV s}^{-1}$  under different bending degree. Adapted from Ref. [84].

of inks was close to the previously reported high-concentration multilayered  $\text{Ti}_3\text{C}_2\text{T}_x$  [94], indicating that the  $\text{Ti}_3\text{C}_2\text{T}_x$  with a high length-to-thickness ratio was suitable for printing. The rheological property of this ink was deeply studied in this work. The shear-thinning behavior of the inks is showed in Fig. 8b. With the shearing force changing, the viscosity decreased at  $1000 \text{ s}^{-1}$  and recovered at  $0.01 \text{ s}^{-1}$ , showing the inks could be extruded under high shearing force and solidified well after printing. Meanwhile, the viscoelasticity of inks with different concentrations (15, 30, and  $50 \text{ mg mL}^{-1}$ ) was also studied. For the inks of  $50 \text{ mg mL}^{-1}$ , the great elastic modulus (36,507 Pa) and yield stress (206 Pa) were also obtained (Fig. 8c). The fabricating process is shown in Fig. 8a and the printed electrode filaments with porous internal structures were prepared (Fig. 8d and e), between which ions could be efficiently transported to achieve high power density. The fabricated MSC with finger thicknesses of  $326 \mu\text{m}$  and gaps of  $187 \mu\text{m}$  showed an ideal capacitive behavior (Fig. 8f) and outstanding cycling life after 10,000 testing at  $1 \text{ A g}^{-1}$  (Fig. 8g). It also showed excellent electrochemical

performance under different current densities (Fig. 8h). In addition to the special layered structure and high electrical conductivity of MXenes, the great hydrophilicity makes it easy to be dispersed in aqueous, which is significant for printing electrode inks. However,  $\text{Ti}_3\text{C}_2\text{T}_x$  is easily oxidized in aqueous, which leads to the structural degradation of  $\text{Ti}_3\text{C}_2\text{T}_x$  [95]. The poor chemical stability of  $\text{Ti}_3\text{C}_2\text{T}_x$  hinders their sustainable storage and application. Wu et al. [23] developed a stable  $\text{Ti}_3\text{C}_2\text{T}_x$  with sodium ascorbate (SA-MXene) as electrode materials for 3D printing supercapacitor.  $\text{Ti}_3\text{C}_2\text{T}_x$  was treated with different materials, and it was found that the SA-MXene material treated by ascorbate ion featured the best oxidation resistance. The good stability of  $\text{Ti}_3\text{C}_2\text{T}_x$  in the air and aqueous was of great significance to 3D printing inks. The SA-MXene inks were printed on A4 paper to fabricate interdigital structure electrodes. After the electrode was vacuum dried, a uniform PVA- $\text{H}_2\text{SO}_4$  gel solution was poured onto the electrodes to obtain a solid MSC. Although without a current collector, the electrode printed on the paper showed high conductivity of  $119 \text{ S cm}^{-1}$ . After 4000 cycles tested



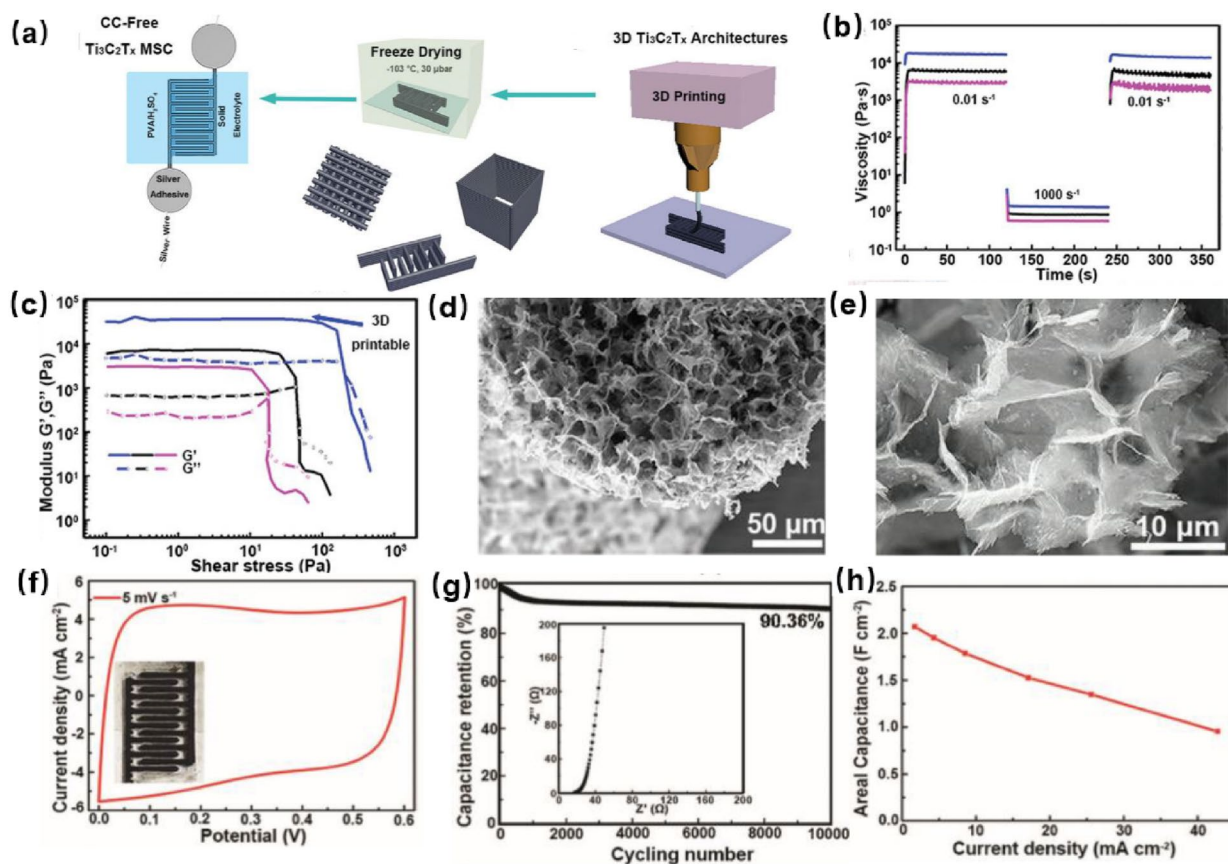


**Figure 8:** (a) Schematic illustration of the fabrication process of the  $\text{Ti}_3\text{C}_2\text{T}_x$  MSC. (b) Inks ( $15, 30,$  and  $50 \text{ mg mL}^{-1}$ ) viscosity evolution over time at  $0.01 \text{ s}^{-1}$  and  $1000 \text{ s}^{-1}$  showcasing viscosity drop and recovery. (c) Storage ( $G'$ ) and loss moduli ( $G''$ ) in terms of shear stress for  $\text{Ti}_3\text{C}_2\text{T}_x$  inks with different concentrations ( $15, 30,$  and  $50 \text{ mg mL}^{-1}$ ). (d, e) The SEM images of printed filaments with porous internal structures after freeze-drying. (f) CV curves at  $5 \text{ mV s}^{-1}$ . (g) Cycling performance at  $1 \text{ A g}^{-1}$  after 10,000 cycles. (h) Areal capacitance at  $2\text{--}44 \text{ mA cm}^{-2}$ . Adapted from Ref. [93].

at a current density of  $1 \text{ A g}^{-1}$ , the prepared MSC still exhibited a capacitance retention of 94.7%.

Nanowires feature large surface area, direct conductive pathways and controllable aspect ratio, also have great advantages in the construction of high-performance electrodes. Yang et al. [96] constructed asymmetric supercapacitors with high nanowire mass, which provided massive electrochemical reaction area and fast electron/ion transport path, thus achieving superior energy and power density. Compared with a symmetrical supercapacitor, the asymmetric supercapacitor has a higher voltage window, resulting in higher energy density. Traditional symmetrical supercapacitors are composed of electrodes with the same type of electrode material and the mass load, which means that the stable potential window of supercapacitors only covers the narrow potential range of a single type of active material. Asymmetric supercapacitors are generally divided into two types, namely two capacitive electrodes system or hybrid capacitors system. For hybrid capacitors, one electrode stores the charge through the battery-type Faradaic process, while the other electrode stores the charge based on the capacitive mechanism. The

voltage window of asymmetric supercapacitor devices could be maximized by the different potential windows of the two electrodes [97]. Shen et al. [58] printed quasi-solid-state asymmetric supercapacitors using vanadium pentoxide ( $\text{V}_2\text{O}_5$ ) and graphene-vanadium nitride quantum dots (G-VNQDs) as the cathode and anode active materials, respectively. The viscosities of electrode inks decreased linearly with the increase of shear rate, indicating good shear-thinning ability. The areal and volumetric capacitance were respectively  $207.9 \text{ mF cm}^{-2}$  and  $5.0 \text{ F cm}^{-3}$  with a long cycling life of 8000 cycles.

Tremendous efforts have been devoted to optimizing the electrode materials of 3D-printed supercapacitors [98]. Nevertheless, to prepare a more accurate microdevice and reduce the gap between fingers in the manufacturing process, some new technologies have also been applied. Electrohydrodynamic (EHD) jet printing technology can be used to print high-resolution patterns, which is expected to be promising in fabricating microdevices [99]. Lee et al. [100] utilized EHD jet printing technology for the first time in MSC. The interdigital electrodes with a very narrow width ( $10 \mu\text{m}$ ) were printed. Distilled water

and alcohol were mainly used as the solvent in preparing electrode inks, and activated carbon, carboxymethyl cellulose, super-P was used as other additives, while the UV-cured thiolene acted as a solid-state gel electrolyte. Moreover, a nozzle with an inner diameter of 10  $\mu\text{m}$  was used in the printing process, and active particles with a small size (64.15 nm) were selected to prevent nozzle clogging. The MSC with an electrode width of 10  $\mu\text{m}$  exhibited the areal capacitance of 127.5  $\mu\text{F cm}^{-2}$  at 1  $\text{mV s}^{-1}$ .

Supercapacitors can be quickly charged/discharged in seconds and can maintain high capacitance after even tens of thousands of cycles. However, the energy density of supercapacitors is still unsatisfactory. Increasing the mass loading of active substances can effectively improve the areal capacitance of supercapacitors. In general, with the increase of the load, the thickness of the electrode will also increase, which leads to the slow diffusion of ions. MSC can well overcome this limitation of the thick electrode. However, the effect of subtle microstructure inside the electrode on electrochemical properties needs to be further researched. For example, the electrode layers of 3D scaffolds are usually stacked in a sequence to form porous structure. The porous design of other structures has certain Reference significance for interdigital structures. Yao et al. [101] developed a 3D-printed graphene aerogel electrode with a high loading of manganese dioxide ( $\text{MnO}_2$ ). This electrode with porous structures could be increased to 4 mm without sacrificing electrochemical performance. The  $\text{MnO}_2$  was deposited onto the graphene aerogel skeleton with a reasonable lattice structure, which not only occurred on the surface of the framework but also inside it. Thereby an ultra-high areal density (1.56  $\text{mWh cm}^{-2}$ ) was obtained. This work provides a new method for the preparation of energy storage devices with high mass loading and high energy density, which was inspiring for designing

similar microstructure during fabricating interdigital electrodes. 3D-printed interdigital supercapacitors need to retain high capacitance while being miniaturized. The careful regulation of pore size and microstructure is the key factor to improve the energy density of micro-supercapacitors. 3D-printed interdigital supercapacitor with higher performance is expected in the future. Table 3 summarizes the materials and electrochemical performances referring to recently published papers about printed interdigital supercapacitors.

## Summary and outlooks

In this review, we have introduced several 3D printing methods commonly used in printing interdigital electrodes, as well as the basic materials for electrode, electrolyte, current collector, and packaging materials. Then the latest progress in 3D-printed interdigital batteries and supercapacitors are highlighted. Compared with the traditional manufacturing process, 3D printing techniques have great potential in manufacturing micro-EES devices with complex structures. The high-integrated micro-interdigital EES devices can provide high operating voltage and energy density, and a narrow interdigital electrode gap brings faster ion diffusion. Interdigital batteries or supercapacitors printed with 3D printing techniques show great potential in various electronic systems. However, there are still many challenges in the preparation of 3D-printed interdigital EES devices.

First, there are few suitable ink materials, especially many active materials that are not suitable for printing. Qualified printing ink should have proper rheological property. At present, additives will be added into the inks to regulate the rheological properties. However, additional additives will usually affect the composition of the electrode materials, thereby affecting its

**TABLE 3:** Various types of inks prescribed and the electrochemical performances of the printed interdigital supercapacitors.

Cathode/anode	Electrolyte	Specific capacity	Energy/power density	References
MXene-AgNW-MONW-C60	PVA-KOH	216.2 $\text{mF cm}^{-2}$ at 10 $\text{mV s}^{-1}$	19.2 $\mu\text{Wh cm}^{-2}$ at 0.86 $\text{mW cm}^{-2}$	[84]
( $\text{VO}_x\text{-rGO}$ )/(G-VNQDs-rGO)	PVA-LiCl	207.9 $\text{mF cm}^{-2}$	73.9 $\mu\text{Wh cm}^{-2}$ and 3.77 $\text{mW cm}^{-2}$	[58]
$\text{Ti}_3\text{C}_2\text{T}_x$	PVA- $\text{H}_2\text{SO}_4$	2.1 $\text{F cm}^{-2}$ at 1.7 $\text{mA cm}^{-2}$ /242.5 $\text{F g}^{-1}$ at 0.2 $\text{A g}^{-1}$	0.0244 $\text{mWh cm}^{-2}$ at 0.64 $\text{mW cm}^{-2}$	[93]
CNT-PANI	PVA- $\text{H}_3\text{PO}_4$	167 $\text{mF cm}^{-2}$ at 0.4 $\text{mA cm}^{-2}$	14.9 $\mu\text{Wh cm}^{-2}$ at 0.29 $\text{mW cm}^{-2}$	[83]
SA-MXene	PVA- $\text{H}_2\text{SO}_4$	108.1 $\text{mF cm}^{-2}$ at 1 $\text{A g}^{-1}$	100.2 $\text{mWh cm}^{-3}$ at 1.9 $\text{W cm}^{-3}$	[23]
Ni-Co-O-GO/ $\text{MnO}_2$ -GO	PVA-KOH	384.9 $\text{mF cm}^{-2}$	90 $\text{mW h cm}^{-2}$	[102]
$\text{Cu}_{0.56}\text{Co}_{2.44}\text{O}_4$ @ $\text{MnO}_2$ /CNT	PVA-KON	665.3 $\text{mF cm}^{-2}$ at 3.2 $\text{mA cm}^{-2}$	182.3 $\mu\text{Wh cm}^{-2}$ at 2.3 $\text{mW cm}^{-2}$	[103]
$\text{Ti}_3\text{C}_2\text{T}_x$	PVA- $\text{H}_2\text{SO}_4$	1035 $\text{mF cm}^{-2}$ at 2 $\text{mV s}^{-1}$	51.7 $\mu\text{Wh cm}^{-2}$ and 5.7 $\text{mW cm}^{-2}$	[87]
PANI-rGO	PVA- $\text{H}_2\text{SO}_4$	1255 $\text{mF cm}^{-2}$ at 4.2 $\text{mA cm}^{-2}$		[104]
$\text{MoO}_3\text{-x}$ /carbon nanospheres	PVA- $\text{H}_3\text{PO}_4$	47.20 $\text{mF cm}^{-2}$ at 10 $\text{mA cm}^{-2}$	21.20 $\mu\text{Wh cm}^{-2}$ at 0.18 $\text{mW cm}^{-2}$	[105]
MOF-199@ZIF-67	$\text{H}_2\text{SO}_4$	5.02 $\text{mF cm}^{-2}$ at 0.2 $\text{mA cm}^{-2}$		[86]
$\text{Fe}_2\text{O}_3$ -graphene-Ag	PVA-LiCl	412.3 $\text{mF cm}^{-2}$ at 2 $\text{mA cm}^{-2}$	65.4 $\mu\text{Wh cm}^{-2}$ at 1.07 $\text{mW cm}^{-2}$	[106]
HGO- $\text{Co}_3\text{O}_4$	PVA-KOH	241.3 $\text{mF cm}^{-2}$ at 2 $\text{mV s}^{-1}$		[107]
$\text{NiO@rGO}$	PVA-KOH	400.3 $\text{F g}^{-1}$		[108]

electrochemical performance. To obtain high electrochemical performance, the exploration of more appropriate inks components of various active materials is inevitable. Meanwhile, the printed electrode and electrolyte with the customized structure are often obtained by extra steps such as heat treatment and freeze-drying, which leads to a complicated preparation process and high cost. Therefore, the further optimization of post-processing methods is important for to the practical production of micro-EES devices.

Second, common 3D printing methods have their own shortcomings in constructing micro/submicro-scale structures. For interdigital electrodes, DIW, SLA, and other techniques can be used to print electrodes with extremely narrow gaps, and electrolytes can be accurately printed in the gaps to prepare solid-state devices with high energy density. The printed electrodes with a more subtle microstructure will further improve the electrochemical performance of devices. However, although interdigital electrodes with appropriate width and electrode gaps can greatly improve the performance of EES devices, the existing design of interdigital structure is still limited in mesoscopic. There are still some obstacles in printing high-precision structures. The reason is that the composition and rheological properties of inks will affect the formation of microscopic 3D architecture and the resolution of current 3D printing technology does not meet the requirement of higher-precision structure. Co-integration of the manufacturing method to target material is another challenge for 3D printing of EES devices. For DIW, a variety of active materials can be used as 3D printing ink. DIW can be used to prepare highly loaded 3D complex electrodes. In the future, new materials with porous structures or large specific surface areas may further improve the electrochemical performance of printing electrodes. IJP ink has special requirements in viscosity, the viscosity of ink is generally low to avoid blocking the nozzle in the printing process. Because of the low viscosity of inks, IJP is difficult to print electrode patterns with high load. Nevertheless, IJP can be widely used in the microelectronics industry owing to its facility process. SLA can take full advantage of printing complex structures to prepare solid electrolytes with conformal interfaces, which has great potential in the preparation of large-scale industrial solid electrolytes in the future. SLS has been developed to enable the carbonization of carbonaceous precursors in an efficient manner to obtain high-performance electrode materials. Additionally, 3D printing is a method with stacking characteristics, uneven stress is inevitable to appear between layers, thus leading to the deformation of devices. Further research needs to be conducted to break through this limitation, finally achieving high mechanical properties and flexibility in 3D-printed EES devices.

Third, packaging material can also be printed after the fabrication of devices, which is of positive significance for fully printed EES devices. Especially for highly integrated devices, a

facile packaging strategy is significant. However, more attention is paid to the properties of printed electrodes, there are limited reports about the full-printed EES devices. Therefore, it will be an important direction to systematically study full-printed micro-EES devices.

## Acknowledgments

This work was supported by the National Key Research and Development Program of China (Grant No. 2020YFA715000), the National Natural Science Foundation of China (Grant No. 51802239), the National Key Research and Development Program of China (Grant No. 2019YFA0704902), Foshan Xianhu Laboratory of the Advanced Energy Science and Technology Guangdong Laboratory (Grant Nos. XHT2020-005, XHT2020-003), the Natural Science Foundation of Hubei Province (Grant No. 2019CFA001), the Fundamental Research Funds for the Central Universities (Grant Nos. WUT: 2020III011GX, 2020IVB057, 2019IVB054, 2019III062JL).

## Declarations

**Conflict of interest** On behalf of all authors, the corresponding author states that there is no conflict of interest.

## References

1. T.Q. Trung, N.E. Lee, Flexible and stretchable physical sensor integrated platforms for wearable human-activity monitoring and personal healthcare. *Adv. Mater.* **28**, 4338–4372 (2016). <https://doi.org/10.1002/adma.201504244>
2. Y.F. Guo, S. Chen, L.J. Sun, L. Yang, L.Z. Zhang, J.M. Lou, Z.W. You, Degradable and fully recyclable dynamic thermoset elastomer for 3D-Printed wearable electronics. *Adv. Funct. Mater.* **31**, 2009799 (2020). <https://doi.org/10.1002/adfm.202009799>
3. J.X. Zhao, Y. Zhang, Y.N. Huang, J.X. Xie, X.X. Zhao, C.W. Li, J.Y. Qu, Q.C. Zhang, J. Sun, B. He, Q.L. Li, C.H. Lu, X.H. Xu, W.B. Lu, L.Q. Li, Y.G. Yao, 3D printing fiber electrodes for an all-fiber integrated electronic device via hybridization of an asymmetric supercapacitor and a temperature sensor. *Adv. Sci.* **5**, 1801114 (2018). <https://doi.org/10.1002/advs.201801114>
4. Z.L. Wang, Toward self-powered sensor networks. *Nano Today* **5**, 512–514 (2010). <https://doi.org/10.1016/j.nantod.2010.09.001>
5. Y. Khan, A.E. Ostfeld, C.M. Lochner, A. Pierre, A.C. Arias, Monitoring of vital signs with flexible and wearable medical devices. *Adv. Mater.* **28**, 4373–4395 (2016). <https://doi.org/10.1002/adma.201504366>
6. G. Milczarek, O. Inganäs, Renewable cathode materials from biopolymer/conjugated polymer interpenetrating networks. *Science* **335**, 1468 (2012). <https://doi.org/10.1126/science.1218316>



7. G.P. Wang, L. Zhang, J.J. Zhang, A review of electrode materials for electrochemical supercapacitors. *Chem. Soc. Rev.* **41**, 797–828 (2012). <https://doi.org/10.1039/c1cs15060j>
8. M. Pumera, Graphene-based nanomaterials for energy storage. *Energy Environ. Sci.* **4**, 668–674 (2011). <https://doi.org/10.1039/c0ee00295j>
9. Y. Shi, C. Eze, B.Y. Xiong, W.D. He, H. Zhang, T.M. Lim, A. Ukil, J.Y. Zhao, Recent development of membrane for vanadium redox flow battery applications: a review. *Appl. Energy* **238**, 202–224 (2019). <https://doi.org/10.1016/j.apenergy.2018.12.087>
10. K.F. Chen, D.F. Xue, Materials chemistry toward electrochemical energy storage. *J. Mater. Chem. A* **4**, 7522–7537 (2016). <https://doi.org/10.1039/c6ta01527a>
11. N.H. Liu, Y.H. Gao, Recent progress in micro-supercapacitors with in-plane interdigital electrode architecture. *Small* **13**, 1701989 (2017). <https://doi.org/10.1002/smll.201701989>
12. J. Lin, C.G. Zhang, Z. Yan, Y. Zhu, Z.W. Peng, R.H. Hauge, D. Natelson, J.M. Tour, 3-Dimensional graphene carbon nanotube carpet-based microsupercapacitors with high electrochemical performance. *Nano Lett.* **13**, 72–78 (2013). <https://doi.org/10.1021/nl3034976>
13. Z.M. Hao, L. Xu, Q. Liu, W. Yang, X.B. Liao, J.S. Meng, X.F. Hong, L. He, L.Q. Mai, On-chip Ni–Zn microbattery based on hierarchical ordered porous Ni@Ni(OH)<sub>2</sub> microelectrode with ultrafast ion and electron transport kinetics. *Adv. Funct. Mater.* **29**, 1808470 (2019). <https://doi.org/10.1002/adfm.201808470>
14. L. Li, C.W. Fu, Z. Lou, S. Chen, W. Han, K. Jiang, D. Chen, G.Z. Shen, Flexible planar concentric circular micro-supercapacitor arrays for wearable gas sensing application. *Nano Energy* **41**, 261–268 (2017). <https://doi.org/10.1016/j.nanoen.2017.08.060>
15. L.C. Hwa, S. Rajoo, A.M. Noor, N. Ahmad, M.B. Uday, Recent advances in 3D printing of porous ceramics: a review. *Curr. Opin. Solid State Mater. Sci.* **21**, 323–347 (2017). <https://doi.org/10.1016/j.cossms.2017.08.002>
16. W.H. Lai, Y. Wang, Z.W. Lei, R.H. Wang, Z.Y. Lin, C.P. Wong, F.Y. Kang, C. Yang, High performance, environmentally benign and integratable Zn//MnO<sub>2</sub> microbatteries. *J. Mater. Chem. A* **6**, 3933–3940 (2018). <https://doi.org/10.1039/c7ta10936a>
17. G.Q. Sun, X.T. Jin, H.S. Yang, J. Gao, L.T. Qu, An aqueous Zn–MnO<sub>2</sub> rechargeable microbattery. *J. Mater. Chem. A* **6**, 10926–10931 (2018). <https://doi.org/10.1039/c8ta02747a>
18. M. Beidaghi, C.L. Wang, Micro-supercapacitors based on interdigital electrodes of reduced graphene oxide and carbon nanotube composites with ultrahigh power handling performance. *Adv. Funct. Mater.* **22**, 4501–4510 (2012). <https://doi.org/10.1002/adfm.201201292>
19. M. Wei, F. Zhang, W. Wang, P. Alexandridis, C. Zhou, G. Wu, 3D direct writing fabrication of electrodes for electrochemical storage devices. *J. Power Sources* **354**, 134–147 (2017). <https://doi.org/10.1016/j.jpowsour.2017.04.042>
20. S.A.M. Tofail, E.P. Koumoulos, A. Bandyopadhyay, S. Bose, L. O'Donoghue, C. Charitidis, Additive manufacturing: scientific and technological challenges, market uptake and opportunities. *Mater. Today* **21**, 22–37 (2018). <https://doi.org/10.1016/j.mat-tod.2017.07.001>
21. X.J. Gao, Q. Sun, X.F. Yang, J.N. Liang, A. Koo, W.H. Li, J.W. Liang, J.W. Wang, R.Y. Li, F.B. Holness, A.D. Price, S.L. Yang, T.K. Sham, X.L. Sun, Toward a remarkable Li–S battery via 3D printing. *Nano Energy* **56**, 595–603 (2019). <https://doi.org/10.1016/j.nanoen.2018.12.001>
22. R.R. Kohlmeier, A.J. Blake, J.O. Hardin, E.A. Carmona, J. Carpena-Núñez, B.J. Maruyama, J.D. Berrigan, H. Huang, M.F. Durstock, Composite batteries: a simple yet universal approach to 3D printable lithium-ion battery electrodes. *J. Mater. Chem. A* **4**, 16856–16864 (2016). <https://doi.org/10.1039/c6ta07610f>
23. C.W. Wu, B. Unnikrishnan, I.W.P. Chen, S.G. Harroun, H.T. Chang, C.C. Huang, Excellent oxidation resistive MXene aqueous ink for micro-supercapacitor application. *Energy Storage Mater.* **25**, 563–571 (2020). <https://doi.org/10.1016/j.ensm.2019.09.026>
24. Q.M. Chen, R. Xu, Z.T. He, K.J. Zhao, L. Pan, Printing 3D gel polymer electrolyte in lithium-ion microbattery using stereolithography. *J. Electrochem. Soc.* **164**, A1852–A1857 (2017). <https://doi.org/10.1149/2.0651709jes>
25. Q.W. Liu, G.F. Zhang, N. Chen, X.X. Feng, C.Z. Wang, J.Q. Wang, X.T. Jin, L.T. Qu, The first flexible dual-ion microbattery demonstrates superior capacity and ultrahigh energy density. *Adv. Funct. Mater.* **30**, 2002086 (2020). <https://doi.org/10.1002/adfm.202002086>
26. X.C. Tian, J. Jin, S.Q. Yuan, C.K. Chua, S.B. Tor, K. Zhou, Emerging 3D-printed electrochemical energy storage devices: a critical review. *Adv. Energy Mater.* **7**, 1700127 (2017). <https://doi.org/10.1002/aenm.201700127>
27. M.P. Browne, E. Redondo, M. Pumera, 3D printing for electrochemical energy applications. *Chem. Rev.* **120**, 2783–2810 (2020). <https://doi.org/10.1021/acs.chemrev.9b00783>
28. C. Zhang, K. Shen, B. Li, S.M. Li, S.B. Yang, Continuously 3D printed quantum dot-based electrodes for lithium storage with ultrahigh capacities. *J. Mater. Chem. A* **6**, 19960–19966 (2018). <https://doi.org/10.1039/c8ta08559e>
29. P.E. Delannoy, B. Riou, B. Lestriez, D. Guyomard, T. Brousse, J. Le Bideau, Toward fast and cost-effective ink-jet printing of solid electrolyte for lithium microbatteries. *J. Power Sources* **274**, 1085–1090 (2015). <https://doi.org/10.1016/j.jpowsour.2014.10.164>
30. M.P. Down, E. Martínez-Periñán, C.W. Foster, E. Lorenzo, G.C. Smith, C.E. Banks, Next-generation additive manufacturing of complete standalone sodium-ion energy storage architectures. *Adv. Energy Mater.* **9**, 1803019 (2019). <https://doi.org/10.1002/aenm.201803019>

31. K. Fu, Y.G. Yao, J.Q. Dai, L.B. Hu, Progress in 3D printing of carbon materials for energy-related applications. *Adv. Mater.* **29**, 1603486 (2017). <https://doi.org/10.1002/adma.201603486>
32. A.D. Valentine, T.A. Busbee, J.W. Boley, J.R. Raney, A. Chortos, A. Kotikian, J.D. Berrigan, M.F. Durstock, J.A. Lewis, Hybrid 3D printing of soft electronics. *Adv. Mater.* **29**, 1703817 (2017). <https://doi.org/10.1002/adma.201703817>
33. A. Ambrosi, M. Pumera, 3D-printing technologies for electrochemical applications. *Chem. Soc. Rev.* **45**, 2740–2755 (2016). <https://doi.org/10.1039/c5cs00714c>
34. J. Malda, J. Visser, F.P. Melchels, T. Jungst, W.E. Hennink, W.J.A. Dhert, J. Groll, D.W. Hutmacher, 25th anniversary article: engineering hydrogels for biofabrication. *Adv. Mater.* **25**, 5011–5028 (2013). <https://doi.org/10.1002/adma.201302042>
35. J.A. Lewis, Direct ink writing of 3D functional materials. *Adv. Funct. Mater.* **16**, 2193–2204 (2006). <https://doi.org/10.1002/adfm.200600434>
36. M. Singh, H.M. Haverinen, P. Dhagat, G.E. Jabbour, Inkjet printing-process and its applications. *Adv. Mater.* **22**, 673–685 (2010). <https://doi.org/10.1002/adma.200901141>
37. K.H. Choi, J. Yoo, C.K. Lee, S.Y. Lee, All-inkjet-printed, solid-state flexible supercapacitors on paper. *Energy Environ. Sci.* **9**, 2812–2821 (2016). <https://doi.org/10.1039/c6ee00966b>
38. H.D. Wu, W. Liu, R.X. He, Z.W. Wu, Q.G. Jiang, X. Song, Y. Chen, L.X. Cheng, S.H. Wu, Fabrication of dense zirconia-toughened alumina ceramics through a stereolithography-based additive manufacturing. *Ceram. Int.* **43**, 968–972 (2017). <https://doi.org/10.1016/j.ceramint.2016.10.027>
39. F.P.W. Melchels, J. Feijen, D.W. Grijpma, A review on stereolithography and its applications in biomedical engineering. *Biomaterials* **31**, 6121–6130 (2010). <https://doi.org/10.1016/j.biomaterials.2010.04.050>
40. I. Gibson, D.P. Shi, Material properties and fabrication parameters in selective laser sintering process. *Rapid Prototyping J.* **3**, 129–136 (1997). <https://doi.org/10.1108/13552549710191836>
41. J. Bauer, A. Schroer, R. Schwaiger, O. Kraft, Approaching theoretical strength in glassy carbon nanolattices. *Nat. Mater.* **15**, 438–443 (2016). <https://doi.org/10.1038/nmat4561>
42. M. Cheng, R. Deivanayagam, R. Shahbazian-Yassar, 3D printing of electrochemical energy storage devices: a review of printing techniques and electrode/electrolyte architectures. *Batteries Supercaps.* **3**, 130–146 (2020). <https://doi.org/10.1002/batt.201900130>
43. M. Regehly, Y. Garmshausen, M. Reuter, N.F. Konig, E. Israel, D.P. Kelly, C.Y. Chou, K. Koch, B. Asfari, S. Hecht, Xolography for linear volumetric 3D printing. *Nature* **588**, 620–624 (2020). <https://doi.org/10.1038/s41586-020-3029-7>
44. X.C. Tian, K. Zhou, 3D printing of cellular materials for advanced electrochemical energy storage and conversion. *Nanoscale* **12**, 7416–7432 (2020). <https://doi.org/10.1039/d0nr00291g>
45. J.J. Huang, J.J. Yang, W.R. Li, W.B. Cai, Z.Y. Jiang, Electrochemical properties of LiCoO<sub>2</sub> thin film electrode prepared by ink-jet printing technique. *Thin Solid Films* **516**, 3314–3319 (2008). <https://doi.org/10.1016/j.tsf.2007.09.039>
46. Y.B. Wang, C.J. Chen, H. Xie, T.T. Gao, Y.G. Yao, G. Pastel, X.G. Han, Y.J. Li, J.P. Zhao, K. Fu, L.B. Hu, 3D-printed all-fiber Li-ion battery toward wearable energy storage. *Adv. Funct. Mater.* **27**, 1703140 (2017). <https://doi.org/10.1002/adfm.201703140>
47. K. Fu, Y.B. Wang, C.Y. Yan, Y.G. Yao, Y.N. Chen, J.Q. Dai, S. Lacey, Y.B. Wang, J.Y. Wan, T. Li, Z.Y. Wang, Y. Xu, L.B. Hu, Graphene oxide-based electrode inks for 3D-printed lithium-ion batteries. *Adv. Mater.* **28**, 2587–2594 (2016). <https://doi.org/10.1002/adma.201505391>
48. X.F. Lu, T.K. Zhao, X.L. Ji, J.T. Hu, T.H. Li, X. Lin, W.D. Huang, 3D printing well organized porous iron-nickel/polyaniline nanocages multiscale supercapacitor. *J. Alloys Compd.* **760**, 78–83 (2018). <https://doi.org/10.1016/j.jallcom.2018.05.165>
49. J.T. Hu, Y. Jiang, S.H. Cui, Y.D. Duan, T.C. Liu, H. Guo, L.P. Lin, Y. Lin, J.X. Zheng, K. Amine, F. Pan, 3D-printed cathodes of LiMn<sub>1-x</sub>Fe<sub>x</sub>PO<sub>4</sub> nanocrystals achieve both ultrahigh rate and high capacity for advanced lithium-ion battery. *Adv. Energy Mater.* **6**, 1600856 (2016). <https://doi.org/10.1002/aenm.201600856>
50. J.S. Cai, Z.D. Fan, J. Jin, Z.X. Shi, S.X. Dou, J.Y. Sun, Z.F. Liu, Expediting the electrochemical kinetics of 3D-printed sulfur cathodes for Li-S batteries with high rate capability and areal capacity. *Nano Energy* **75**, 104970 (2020). <https://doi.org/10.1016/j.nanoen.2020.104970>
51. S.D. Lacey, D.J. Kirsch, Y.J. Li, J.T. Morgenstern, B.C. Zarket, Y.G. Yao, J.Q. Dai, L.Q. Garcia, B.Y. Liu, T.T. Gao, S.M. Xu, S.R. Raghavan, J.W. Connell, Y. Lin, L.B. Hu, Extrusion-based 3D printing of hierarchically porous advanced battery electrodes. *Adv. Mater.* **30**, e1705651 (2018). <https://doi.org/10.1002/adma.201705651>
52. A. Maurel, M. Courty, B. Fleutot, H. Tortajada, K. Prashantha, M. Armand, S. Grugeon, S. Panier, L. Dupont, Highly loaded graphite-poly(lactic acid) composite-based filaments for lithium-ion battery three-dimensional printing. *Chem. Mater.* **30**, 7484–7493 (2018). <https://doi.org/10.1021/acs.chemmater.8b02062>
53. S.Y. Lin, Y.J. Zhong, X.L. Zhao, T. Sawada, X.M. Li, W.H. Lei, M.R. Wang, T. Serizawa, H.W. Zhu, Synthetic multifunctional graphene composites with reshaping and self-healing features via a facile biomineralization-inspired process. *Adv. Mater.* **30**, 1803004 (2018). <https://doi.org/10.1002/adma.201803004>
54. D.X. Cao, Y.J. Xing, K. Tantratian, X. Wang, Y. Ma, A. Mukhopadhyay, Z. Cheng, Q. Zhang, Y.C. Jiao, L. Chen, H.L. Zhu, 3D printed high-performance lithium metal microbatteries

- enabled by nanocellulose. *Adv. Mater.* **31**, 1807313 (2019). <https://doi.org/10.1002/adma.201807313>
55. Y. Chen, Z.Y. Yu, Y.H. Ye, Y.F. Zhang, G.Y. Li, F. Jiang, Super-elastic, hygroscopic, and ionic conducting cellulose nanofibril monoliths by 3D printing. *ACS Nano* **15**, 1869–1879 (2021). <https://doi.org/10.1021/acsnano.0c10577>
  56. J.H. Kim, S. Lee, M. Wajahat, H. Jeong, W.S. Chang, H.J. Jeong, J.R. Yang, J.T. Kim, S.K. Seol, Three-dimensional printing of highly conductive carbon nanotube microarchitectures with fluid ink. *ACS Nano* **10**, 8879–8887 (2016). <https://doi.org/10.1021/acsnano.6b04771>
  57. Y.Q. Liu, B.B. Zhang, Q. Xu, Y.Y. Hou, S.Y. Seyedin, S. Qin, G.G. Wallace, S. Beirne, J.M. Razal, J. Chen, Development of graphene oxide/polyaniline inks for high performance flexible microsupercapacitors via extrusion printing. *Adv. Funct. Mater.* **28**, 1706592 (2018). <https://doi.org/10.1002/adfm.201706592>
  58. K. Shen, J.W. Ding, S.B. Yang, 3D printing quasi-solid-state asymmetric micro-supercapacitors with ultrahigh areal energy density. *Adv. Energy Mater.* **8**, 1800408 (2018). <https://doi.org/10.1002/aenm.201800408>
  59. H. Gao, K. Lian, Proton-conducting polymer electrolytes and their applications in solid supercapacitors: a review. *RSC Adv.* **4**, 33091–33113 (2014). <https://doi.org/10.1039/c4ra05151c>
  60. Z.Y. Xu, C.C. Fan, Q. Zhang, Y. Liu, C.Y. Cui, B. Liu, T.L. Wu, X.P. Zhang, W.G. Liu, A self-thickening and self-strengthening strategy for 3D printing high-strength and anti-swelling supramolecular polymer hydrogels as meniscus substitutes. *Adv. Funct. Mater.* (2021). <https://doi.org/10.1002/adfm.202100462>
  61. L.G. Bettini, P. Piseri, F. De Giorgio, C. Arbizzani, P. Milani, F. Soavi, Flexible, ionic liquid-based micro-supercapacitor produced by supersonic cluster beam deposition. *Electrochim. Acta* **170**, 57–62 (2015). <https://doi.org/10.1016/j.electacta.2015.04.068>
  62. B. Yiming, Y. Han, Z. Han, X. Zhang, Y. Li, W. Lian, M. Zhang, J. Yin, T. Sun, Z. Wu, T. Li, J. Fu, Z. Jia, S. Qu, A mechanically robust and versatile liquid-free ionic conductive elastomer. *Adv. Mater.* **33**, 2006111 (2021). <https://doi.org/10.1002/adma.202006111>
  63. M. Cheng, Y.Z. Jiang, W.T. Yao, Y.F. Yuan, R. Deivanayagam, T. Foroozan, Z.N. Huang, B.A. Song, R. Rojaee, T. Shokuhfar, Y. Pan, J. Lu, R. Shahbazian-Yassar, Elevated-temperature 3D printing of hybrid solid-state electrolyte for Li-ion batteries. *Adv. Mater.* **30**, 1800615 (2018). <https://doi.org/10.1002/adma.201800615>
  64. S.H. Kim, C.H. Choi, S.J. Cho, J.T. Yoo, S.S. Lee, S.Y. Lee, Flexible/shape-versatile, bipolar all-solid-state lithium-ion batteries prepared by multistage printing. *Energy Environ. Sci.* **11**, 321–330 (2018). <https://doi.org/10.1039/c7ee01630a>
  65. L.X. Feng, K. Wang, X. Zhang, X.Z. Sun, C. Li, X.B. Ge, Y.W. Ma, Flexible solid-state supercapacitors with enhanced performance from hierarchically graphene nanocomposite electrodes and ionic liquid incorporated gel polymer electrolyte. *Adv. Funct. Mater.* **28**, 1704463 (2018). <https://doi.org/10.1002/adfm.201704463>
  66. S. Zekoll, C. Marriner-Edwards, A.K.O. Hekselman, J. Kasem-chainan, C. Kuss, D.E.J. Armstrong, D.Y. Cai, R.J. Wallace, F.H. Richter, J.H.J. Thijssen, P.G. Bruce, Hybrid electrolytes with 3D bicontinuous ordered ceramic and polymer microchannels for all-solid-state batteries. *Energy Environ. Sci.* **11**, 185–201 (2018). <https://doi.org/10.1039/c7ee02723k>
  67. D.W. McOwen, S. Xu, Y. Gong, Y. Wen, G.L. Godbey, J.E. Gritton, T.R. Hamann, J. Dai, G.T. Hitz, L. Hu, E.D. Wachsman, 3D-printing electrolytes for solid-state batteries. *Adv. Mater.* **30**, 1707132 (2018). <https://doi.org/10.1002/adma.201707132>
  68. C.J. Chae, J.H. Han, S.S. Lee, Y.M. Choi, T.H. Kim, S.H. Jeong, A printable metallic current collector for all-printed high-voltage micro-supercapacitors: instantaneous surface passivation by flash-light-sintering reaction. *Adv. Funct. Mater.* **30**, 2000715 (2020). <https://doi.org/10.1002/adfm.202000715>
  69. L. Liu, Q. Lu, S.L. Yang, J. Guo, Q.Y. Tian, W.J. Yao, Z.H. Guo, V.A.L. Roy, W. Wu, All-printed solid-state microsupercapacitors derived from self-template synthesis of ag@ppy nanocomposites. *Adv. Mater. Technol.* **3**, 1700206 (2018). <https://doi.org/10.1002/admt.201700206>
  70. B.H. Xie, Y. Wang, W.H. Lai, W. Lin, Z.Y. Lin, Z.X. Zhang, P.C. Zou, Y. Xu, S. Zhou, C. Yang, F.Y. Kang, C.P. Wong, Laser-processed graphene based micro-supercapacitors for ultrathin, rollable, compact and designable energy storage components. *Nano Energy* **26**, 276–285 (2016). <https://doi.org/10.1016/j.nanoen.2016.04.045>
  71. B.L. Chen, Y.Z. Jiang, X.H. Tang, Y.Y. Pan, S. Hu, Fully packaged carbon nanotube supercapacitors by direct ink writing on flexible substrates. *ACS Appl. Mater. Interfaces* **9**, 28433–28440 (2017). <https://doi.org/10.1021/acsmi.7b06804>
  72. T.S. Wei, B.Y. Ahn, J. Grotto, J.A. Lewis, 3D printing of customized Li-ion batteries with thick electrodes. *Adv. Mater.* **30**, 1703027 (2018). <https://doi.org/10.1002/adma.201703027>
  73. Y. Liu, Y. Qiao, Y. Zhang, Z. Yang, T.T. Gao, D. Kirsch, B.Y. Liu, J.W. Song, B. Yang, L.B. Hu, 3D printed separator for the thermal management of high-performance Li metal anodes. *Energy Storage Mater.* **12**, 197–203 (2018). <https://doi.org/10.1016/j.ensm.2017.12.019>
  74. K. Sun, T.S. Wei, B.Y. Ahn, J.Y. Seo, S.J. Dillon, J.A. Lewis, 3D printing of interdigitated Li-ion microbattery architectures. *Adv. Mater.* **25**, 4539–4543 (2013). <https://doi.org/10.1002/adma.201301036>
  75. K. Shen, Z.J. Cao, Y.Z. Shi, Y.Z. Zhang, B. Li, S.B. Yang, 3D printing lithium salt towards dendrite-free lithium anodes. *Energy Storage Mater.* **35**, 108–113 (2021). <https://doi.org/10.1016/j.ensm.2020.11.022>



76. W.Y. Wu, J. Duan, J.Y. Wen, Y.W. Chen, X.Y. Liu, L.Q. Huang, Z.F. Wang, S.Y. Deng, Y.H. Huang, W. Luo, A writable lithium metal ink. *Sci. China Chem.* **63**, 1483–1489 (2020). <https://doi.org/10.1007/s11426-020-9810-1>
77. V.G. Rocha, E. Garcia-Tunon, C. Botas, F. Markoulidis, E. Feilden, E. D'Elia, N. Ni, M. Shaffer, E. Saiz, Multimerial 3D printing of graphene-based electrodes for electrochemical energy storage using thermoresponsive inks. *ACS Appl. Mater. Interfaces* **9**, 37136–37145 (2017). <https://doi.org/10.1021/acsmi.7b10285>
78. J.Y. Wu, Z.X. Rao, Z.X. Cheng, L.X. Yuan, Z. Li, Y.H. Huang, Ultrathin, flexible polymer electrolyte for cost-effective fabrication of all-solid-state lithium metal batteries. *Adv. Energy Mater.* **9**, 1902767 (2019). <https://doi.org/10.1002/aenm.201902767>
79. M. Cheng, A. Ramasubramanian, M.G. Rasul, Y.Z. Jiang, Y.F. Yuan, T. Foroozan, R. Deivanayagam, M.T. Saray, R. Rojaee, B. Song, V.R. Yurkiv, Y.Y. Pan, F. Mashayek, R. Shahbazian-Yassar, Direct ink writing of polymer composite electrolytes with enhanced thermal conductivities. *Adv. Funct. Mater.* **31**, 2006683 (2020). <https://doi.org/10.1002/adfm.202006683>
80. M.Y. Yan, Y.L. Zhao, L.Q. Mai, Track batteries degrading in real time. *Nature* **546**, 469 (2017). <https://doi.org/10.1038/546469a>
81. M. Drews, S. Tepner, P. Habertzettl, H. Gentscher, W. Beichel, M. Breitwieser, S. Vierrath, D. Biro, Towards 3D-lithium ion microbatteries based on silicon/graphite blend anodes using a dispenser printing technique. *RSC Adv.* **10**, 22440–22448 (2020). <https://doi.org/10.1039/d0ra03161e>
82. J.X. Zhao, H.Y. Lu, Y. Zhang, S.X. Yu, O.I. Malvi, X.X. Zhao, L.T. Wang, H.B. Wang, J.H. Peng, X.F. Li, Y.Y. Zhang, S. Chen, H. Pan, G.C. Xing, C.H. Lu, Y.X. Tang, X.D. Chen, Direct coherent multi-ink printing of fabric supercapacitors. *Sci. Adv.* **7**, eabd6978 (2021). <https://doi.org/10.1126/sciadv.abd6978>
83. V. Rajendran, A.M.V. Mohan, M. Jayaraman, T. Nakagawa, All-printed, interdigitated, freestanding serpentine interconnects based flexible solid state supercapacitor for self powered wearable electronics. *Nano Energy* **65**, 104055 (2019). <https://doi.org/10.1016/j.nanoen.2019.104055>
84. X.R. Li, H.P. Li, X.Q. Fan, X.L. Shi, J.J. Liang, 3D-printed stretchable micro-supercapacitor with remarkable areal performance. *Adv. Energy Mater.* **10**, 1903794 (2020). <https://doi.org/10.1002/aenm.201903794>
85. Y.M. Chen, M.H. Guo, L. He, W. Yang, L. Xu, J.S. Meng, X.C. Tian, X.Y. Ma, Q. Yu, K. Yang, X. Hong, L. Mai, Scalable microfabrication of three-dimensional porous interconnected graphene scaffolds with carbon spheres for high-performance all carbon-based micro-supercapacitors. *J. Mater.* **5**, 303–312 (2019). <https://doi.org/10.1016/j.jmat.2018.11.009>
86. W. Zhang, R. Li, H. Zheng, J.S. Bao, Y.J. Tang, K. Zhou, Laser-assisted printing of electrodes using metal-organic frameworks for micro-supercapacitors. *Adv. Funct. Mater.* (2021). <https://doi.org/10.1002/adfm.202009057>
87. J. Orangi, F. Hamade, V.A. Davis, M. Beidaghi, 3D printing of additive-free 2D Ti<sub>3</sub>C<sub>2</sub>T<sub>x</sub> (MXene) ink for fabrication of micro-supercapacitors with ultra-high energy densities. *ACS Nano* **14**, 640–650 (2020). <https://doi.org/10.1021/acsnano.9b07325>
88. Z.D. Fan, J. Jin, Li. Chao, J.S. Cai, C.H. Wei, Y.L. Shao, G.F. Zou, J.Y. Sun, 3D-printed Zn-ion hybrid capacitor enabled by universal divalent cation-gelated additive-free Ti<sub>3</sub>C<sub>2</sub> MXene ink. *ACS Nano* **15**, 3098–3107 (2021). <https://doi.org/10.1021/acsnano.0c09646>
89. L.H. Yu, Z.D. Fan, Y.L. Shao, Z.N. Tian, J.Y. Sun, Z.F. Liu, Versatile N-doped MXene ink for printed electrochemical energy storage application. *Adv. Energy Mater.* **9**, 1901839 (2019). <https://doi.org/10.1002/aenm.201901839>
90. L.H. Yu, W.P. Li, C.H. Wei, Q.F. Yang, Y.L. Shao, J.Y. Sun, 3D Printing of NiCoP/Ti<sub>3</sub>C<sub>2</sub> MXene architectures for energy storage devices with high areal and volumetric energy density. *Nanomicro Lett.* **12**, 143 (2020). <https://doi.org/10.1007/s40820-020-00483-5>
91. W.A. Haider, M. Tahir, L. He, H.A. Mirza, R.Q. Zhu, Y.L. Han, L.Q. Mai, Structural engineering and coupling of two-dimensional transition metal compounds for micro-supercapacitor electrodes. *ACS Cent. Sci.* **6**, 1901–1915 (2020). <https://doi.org/10.1021/acscentsci.0c01022>
92. S.H. Zheng, H. Wang, P. Das, Y. Zhang, Y.X. Cao, J.X. Ma, S.Z. Liu, Z.S. Wu, Multitasking MXene inks enable high-performance printable microelectrochemical energy storage devices for all-flexible self-powered integrated systems. *Adv. Mater.* **33**, 2005449 (2021). <https://doi.org/10.1002/adma.202005449>
93. W. Yang, J. Yang, J.J. Byun, F.P. Moissinac, J. Xu, S.J. Haigh, M. Domingos, M.A. Bissett, R.A.W. Dryfe, S. Barg, 3D printing of freestanding MXene architectures for current-collector-free supercapacitors. *Adv. Mater.* **31**, 1902725 (2019). <https://doi.org/10.1002/adma.201902725>
94. B. Akuzum, K. Maleski, B. Anasori, P. Lelyukh, N.J. Alvarez, E.C. Kumbur, Y. Gogotsi, Rheological characteristics of 2D titanium carbide (MXene) dispersions: a guide for processing MXenes. *ACS Nano* **12**, 2685–2694 (2018). <https://doi.org/10.1021/acsnano.7b08889>
95. C.J. Zhang, S. Pinilla, N. McEvoy, C.P. Cullen, B. Anasori, E. Long, S.H. Park, A. Seral-Ascaso, A. Shmeliov, D. Krishnan, C. Morant, X.H. Liu, G.S. Duesberg, Y. Gogotsi, V. Nicolosi, Oxidation stability of colloidal two-dimensional titanium carbides (MXenes). *Chem. Mater.* **29**, 4848–4856 (2017). <https://doi.org/10.1021/acs.chemmater.7b00745>
96. W. Yang, Y.X. Zhu, Z.F. Jia, L. He, L. Xu, J. Meng, M. Tahir, Z.X. Zhou, X.W. Wang, L.Q. Mai, Interwoven nanowire based on-chip asymmetric microsupercapacitor with high integrability,

- areal energy, and power density. *Adv. Energy Mater.* **10**, 2001873 (2020). <https://doi.org/10.1002/aenm.202001873>
97. Y.L. Shao, M.F. El-Kady, J.Y. Sun, Y.G. Li, Q.H. Zhang, M.F. Zhu, H.Z. Wang, B. Dunn, R.B. Kaner, Design and mechanisms of asymmetric supercapacitors. *Chem. Rev.* **118**, 9233–9280 (2018). <https://doi.org/10.1021/acs.chemrev.8b00252>
  98. W.B. Kang, L. Zeng, S.W. Ling, C.H. Zhang, 3D printed supercapacitors toward trinity excellence in kinetics, energy density, and flexibility. *Adv. Energy Mater.* **11**, 2100020 (2021). <https://doi.org/10.1002/aenm.202100020>
  99. M.S. Onses, E. Sutanto, P.M. Ferreira, A.G. Alleyne, J.A. Rogers, Mechanisms, capabilities, and applications of high-resolution electrohydrodynamic jet printing. *Small* **34**, 4237–4266 (2015). <https://doi.org/10.1002/smll.201500593>
  100. K.H. Lee, S.S. Lee, D.B. Ahn, J. Lee, D. Byun, S.Y. Lee, Ultrahigh areal number density solid-state on-chip microsupercapacitors via electrohydrodynamic jet printing. *Sci. Adv.* **6**, 1692 (2020). <https://doi.org/10.1126/sciadv.aaz1692>
  101. B. Yao, S. Chandrasekaran, J. Zhang, W. Xiao, F. Qian, C. Zhu, E.B. Duoss, C.M. Spadaccini, M.A. Worsley, Y. Li, Efficient 3D printed pseudocapacitive electrodes with ultrahigh MnO<sub>2</sub> loading. *Joule* **3**, 459–470 (2019). <https://doi.org/10.1016/j.joule.2018.09.020>
  102. T. Wang, X.C. Tian, L. Li, L.H. Lu, S. Hou, G.Z. Cao, H.Y. Jin, 3D printing-based cellular microelectrodes for high-performance asymmetric quasi-solid-state micro-pseudocapacitors. *J. Mater. Chem. A* **8**, 1749–1756 (2020). <https://doi.org/10.1039/c9ta11386j>
  103. F. Li, M. Huang, J.H. Wang, J. Qu, Y. Li, L.X. Liu, V.K. Bandari, Y. Hong, B.K. Sun, M.S. Zhu, F. Zhu, Y.X. Zhang, O.G. Schmidt, On-chip 3D interdigital micro-supercapacitors with ultrahigh areal energy density. *Energy Storage Mater.* **27**, 17–24 (2020). <https://doi.org/10.1016/j.ensm.2020.01.008>
  104. Z. Wang, Q.E. Zhang, S. Long, Y. Luo, P. Yu, Z. Tan, J. Bai, B. Qu, Y. Yang, J. Shi, H. Zhou, Z.Y. Xiao, W. Hong, H. Bai, Three-dimensional printing of polyaniline/reduced graphene oxide composite for high-performance planar supercapacitor. *ACS Appl. Mater. Interfaces* **10**, 10437–10444 (2018). <https://doi.org/10.1021/acsami.7b19635>
  105. W. Zhao, L. Wei, Q.G. Fu, X. Guo, High-performance, flexible, solid-state micro-supercapacitors based on printed asymmetric interdigital electrodes and bio-hydrogel for on-chip electronics. *J. Power Sources* **422**, 73–83 (2019). <https://doi.org/10.1016/j.jpowsour.2019.03.021>
  106. K. Tang, H. Ma, Y.J. Tian, Z.X. Liu, H.Y. Jin, S. Hou, K. Zhou, X.C. Tian, 3D printed hybrid-dimensional electrodes for flexible micro-supercapacitors with superior electrochemical behaviours. *Virtual Phys. Prototyp.* **15**, 511–519 (2020). <https://doi.org/10.1080/17452759.2020.1842619>
  107. X.C. Tian, K. Tang, H.Y. Jin, T. Wang, X.W. Liu, W. Yang, Z.C. Zou, S. Hou, K. Zhou, Boosting capacitive charge storage of 3D-printed micro-pseudocapacitors via rational holey graphene engineering. *Carbon* **155**, 562–569 (2019). <https://doi.org/10.1016/j.carbon.2019.08.089>
  108. T. Wang, L. Li, X.C. Tian, H.Y. Jin, K. Tang, S. Hou, H. Zhou, X.H. Yu, 3D-printed interdigitated graphene framework as superior support of metal oxide nanostructures for remarkable micro-pseudocapacitors. *Electrochim. Acta* **319**, 245–252 (2019). <https://doi.org/10.1016/j.electacta.2019.06.163>